Thermochemical Lithosphere Differentiation and Early Earth Tectonics

Fabio A. Capitanio[1], Oliver Nebel[1], Jean-François Moyen[1,2], Peter A. Cawood[1]

[1] School of Earth Atmosphere and Environment, Monash University, Clayton, 3800 Victoria, Australia

[2] Université de Lyon, Laboratoire Magmas et Volcans, UJM-UCA-CNRS-IRD, 23 rue Dr. Paul Michelon, 42023 Saint Etienne

Corresponding author: Fabio A. Capitanio (fabio.capitanio@monash.edu)

Key Points:

- Mantle convection regimes with melt-depletion are investigated for internal heat production ranging from present-day to early Earth values
- Themochemical differentiation of a depleted lithosphere is dominant under early Earth coditions
- New tectonic regimes of the hotter early Earth reconcile with thermal evolution and the geological record

Abstract

What tectonic regimes operated on the early Earth and how these differed from modern plate tectonics remain unresolved questions. We use numerical modelling of mantle convection, melting and melt-depletion to address how the regimes emerge under conditions spanning back from a modern to an early Earth, when internal radiogenic heat was higher. For Phanerozoic values of internal heat, the tectonic regime depends on the ability of the lithosphere to yield and form plate margins. For early Earth internal heat values, the mantle reaches higher temperatures, high-degree depletion and differentiated into a thicker and stiffer lithospheric mantle. This thermochemical differentiation stabilises the lithosphere over a large range of modelled strengths, narrowing the viable tectonic regimes of the early Earth. All the models develop in two stages: an early stage, when

decreasing yield strength favours mobility and depletion, and a later stabilisation, when inherited features remain preserved in the rigid lid. The thick lithosphere reduces surface heat loss and its dependence on mantle temperature, reconciling with the thermal history of the early Earth. When compared to the models, the Archean record of large melting, episodic mobility and plate margin activity, subsequently fossilised in rigid cratons, is best explained by the two-stage evolution of a lithosphere prone to yielding, progressively differentiating and stabilising. Thermochemical differentiation holds the key for the evolution of Earth's tectonics: dehydration stiffening resisted the operation of plate margins preserving lithospheric cores, until its waning, as radioactive heat decays, marks the emergence of stable features of modern plate tectonics.

Plain Language Summary

We use numerical models of planetary convection to simulate the conditions under which the first continents formed in the early Earth. We find that for present-day conditions a thermal cool lithosphere forms atop of a hot mantle, which is recycled in the convection and has stable plate margins, that is mid-oceanic ridges and subduction zones. In a hotter Earth, likely conditions of our planet >3 billion years ago, higher-degree melting and deeper melt extraction left larger volumes of mantle dryer and, therefore, stiffer, than today. This thermochemical differentiation of the mantle conferred stability to its outer layer, resulting in the formation of the first lithosphere on our planet. The emergence of stable, thick lithosphere is key to the interpretation of the sparse record of the early Earth processes in continental cores, called cratons, and to the thermal evolution of the planet, thus far considered "paradoxal".

1. Introduction

The tectonic regime of the Earth is driven by heat loss from its interior and in turn controls the conditions under which features such as topography, atmosphere and life emerge. In the current regime, called mobile or active lid (e.g., Lenardic, 2018), the cold shell of the Earth mobilises, fragments into plates, and forms part of the mantle convection regime, thereby regulating thermal loss, (e.g., Korenaga, 2013). An example of mobile lid regime is modern plate tectonics, with features such as rigid plate motions between stable divergent and convergent margins and

their recycling back into the mantle through subduction. While this regime currently operates on Earth, it is widely accepted that the regime of the Precambrian must have been different, (e.g., Cawood et al., 2018; Gerya, 2014; Lenardic, 2018; Stern, 2018). Evidence of large melt-depletion, stabilisation and thickening are relevant constructive processes in continents in the early Earth (Jordan, 1988), which remain at odds with remnant features of destructive processes such as episodic subduction, mantle plumes impingement and lithosphere foundering (Fischer and Gerya, 2016; Johnson et al., 2014; van Hunen and Moyen, 2012). Therefore, in the early Earth regime, the constructive and destructive processes and their relative occurrence must have been largely different from present-day plate tectonics (Jordan, 1988). Yet, as the geological record is fragmented and incomplete, constraints on the regime of the early Earth and how it evolved to modern plate tectonics, are less stringent (e.g., Lenardic, 2018; Stern, 2018). As a consequence, our understanding of the Precambrian evolution is inconclusive, often contradictory, and remains debated.

Thus far, geodynamics arguments constrained only two possible global tectonic regimes on Earth which do not easily reconcile with the geological record. These regimes are (i) a convecting mantle overlayed by a uniform lid, either stagnant or sluggish lid, and (ii) a mode in which the lithosphere is involved in mantle convection, the active or mobile lid (Lenardic, 2018). The regime is critically defined by the temperature- and stress-dependence of rocks' rheology, with mantle temperatures defining properties such as lithosphere thickness and viscosity, and lower yield strength allowing for margin formation and lithosphere subduction (Moresi and Solomatov, 1998; O'Neill et al., 2007). This theoretical and modelling approach suggests that, under Precambrian conditions, the Earth must have been in a regime of a stagnant or sluggish lid, with subduction at best episodic (Lenardic, 2018; O'Neill et al., 2007; Sleep, 2000; Stern, 2018; van Hunen and Moyen, 2012), while the occurrence of a mobile lid regime is ruled out. This evidence remains at odds with the geological record. Common evidence in Archean cratons such as the Kaapvaal, Pilbara and Superior cratons, points to times of increased lid mobility and crustal evolution, formation through the juxtaposition of different blocks (Van Kranendonk et al., 2007; Zeh et al., 2009), with significant extension and shortening (Bédard and Harris, 2014; Cawood et al., 2009; de Wit et al., 2018; Gardiner et al., 2020; Lamb, 1984). Therefore how the evidence of proto-plate margin reconciles with a sluggish lid regime has remained puzzling.

One limitation of these models consists in the lack of stabilising processes arising from the thermochemical differentiation of the mantle in a hotter Earth. Processes such as large melting, density decrease and rheological transition have been invoked to profoundly impact the evolution of the lithosphere's and its ability to resist recycling and to form craton cores (Arndt et al., 2002; Bickle, 1986; Jordan, 1988). It has been shown that embedding these processes in convection models may explain the duality of the Archean record and the thermal evolution of the Earth (Capitanio et al., 2019b; Korenaga, 2006; Nebel et al., 2018), as well as crustal differentiation (Chowdhury et al., 2017; Fischer and Gerya, 2016; Gerya et al., 2014; Piccolo et al., 2019) and plutonism (Lourenço et al., 2018; Rozel et al., 2017). Yet, the balance of these constructive and destructive features and how these reproduce some key observations remains critical to the understanding of the evolution of Earth's tectonics.

Here, we aim at reconciling early Earth tectonic regimes with their geodynamic context using numerical thermochemical models of convection embedding processes relevant to the formation and stabilisation of the early tectosphere (Bickle, 1986; Jordan, 1988). These processes are captured by melting and melt extraction and the associated stiffening of the mantle residue (Korenaga, 2003). Through varying the lithospheric strengths and internal heat production values that are applicable from the Phanerozoic to the Precambrian (Jaupart et al., 2015), the models reproduce a range of coupled tectonics, mantle temperatures and depletion degrees that are tested against the observed geologic constraints. We found that melting is minor in a present day-like regime and poses no constraint to the viability of the mobile or stagnant lid regimes, which remain controlled by the lithospheric strength. However, in a hotter Archean mantle, thicker portions of depleted, stiffer lithosphere form to stabilise the lid and hamper the development of tectonics features. This occurs in a two-stage evolution: from an early stage, when largest recycling, melting and depletion occur, to a late stage, when the depleted mantle thickens and stabilise, preserving the features previously formed. Mantle temperature, melting and depletion degrees constrained for the Archean are best reproduced under conditions favourable for a mobile lid, allowing the formation of episodic divergent and convergent tectonics and their subsequent preservation in stiff cratonic roots. This regime forms a stagnant lid under characteristic conditions of the mobile lid, therefore we call this regime *lid-and-plate* (Capitanio et al., 2019b). A test against heat budget scaling, supports the idea of a different heat flow-internal temperature relation for the early Earth.

2. Modelling approach

To illustrate the emergence of tectonic features within their large-scale regime, we use numerical models of mantle convection embedding thermochemical differentiation through melt depletion and rheological stiffening. These models reproduce convection regimes with a lid of variable mobility, spanning from a poorly mobile to a highly mobile lid, and yield tectonic features, depletion degrees and mantle temperatures that can be compared to what is observed in cratons. Mantle temperatures in the range of those inferred for the Phanerozoic to the Hadean, up to 130-260 ˚C higher than present day (Herzberg et al., 2010), are reached self-consistently using mixed heating conditions, i.e., bottom heating and internal radiogenic heat production. Key to our modelling strategy is the implementation of a dehydration stiffening rheology (Ito et al., 1999; Korenaga, 2003; Phipps-Morgan, 1997; Wang et al., 2018) during melting of the mantle (Fig. 1, see below). While melting is implemented as in other works (e.g., Fischer and Gerya, 2016; Johnson et al., 2014; Sizova et al., 2015), we focus on the residual mantle, as it undergoes melting and melt extraction. In a hotter mantle, melting and depletion occur to larger depth, thereby differentiating the lithosphere into a thermochemical boundary layer (Korenaga, 2003).

We use a rheological profile to illustrate the role of depletion under a thin lithosphere above a hotter mantle (Fig. 2, see below). Different geotherms with a potential temperature of T_P = 1560 ˚C, a likely value for the Precambrain (Herzberg et al., 2010), mimick the thinning of the boundary layer (Fig. 2A). Large volumes and degree of melting (Fig. 2B) form under thinned lithosphere, where depletion values increase from ~0.2 at ~100 km depth to values in excess of ~0.4 at subcrustal depths of ~20 km. This results in an increase of depleted, stiffer bodies along the depth of the lithosphere (Fig. 2C), reaching viscosities that are ~10^3 times higher, extending throughout the thickness of the lithosphere, from the geotherm's intersection with the solidus. A comparisons between the thermal and thermochemical boundary layers' viscosity profiles, $\eta(T)$ and $\eta(T, F)$ (Fig. 2C, thin and thick lines, respectively), illustrates that the integrated strength of thermomechanical lithosphere is larger. This effect is potentially larger with increasing mantle temperatures, as a larger amount of depeletion is achieved.

2.1. Governing equations and numerical method

Convection is modelled as the flow of a viscous fluid at very low Reynolds number in a two-dimensional Cartesian geometry. We use the geodynamic framework Underworld (Moresi et al., 2007) to solve the equations of conservation of mass, momentum and energy using a Eulerian Finite Element Method with Lagrangian particles embedded in the elements (FEM-PIC). The Lagrangian particles allows for multi-material properties, tracked throughout the history of the model. This is key to the implementation of history-dependent melting and melt-extraction used for the melt depletion-dependent rheology.

The conservation of mass equation, enforcing an incompressibility constraint, is:

$$\nabla \cdot \mathbf{u} = 0 \tag{1}$$

where $\mathbf{u}$ is the velocity vector. The conservation of momentum equation is:

$$\nabla \cdot \boldsymbol{\sigma} = \mathbf{f} \tag{2}$$

with $\boldsymbol{\sigma}$ the stress tensor and $\mathbf{f} = \rho\mathbf{g}$ the force term, ρ the density and $\mathbf{g}$ the gravity. The stress tensor is defined as:

$$\boldsymbol{\sigma} = \boldsymbol{\tau} - p\mathbf{I} \tag{3}$$

where $\boldsymbol{\tau}$ is the deviatoric stress and p the pressure and $\mathbf{I}$ is the identity tensor.

Under the Boussinesq approximation, the conservation of energy equation is:

$$\frac{\partial T}{\partial t} + \mathbf{u}\cdot\nabla T = \kappa\nabla^2 T + H_\mathrm{r} + H_\mathrm{a} \tag{4}$$

with T the temperature, t the time, κ the thermal diffusivity, H_r the radiogenic heat generation rate per unit mass and H_a the adiabatic heating (Turcotte and Schubert, 1982):

$$H_\mathrm{r} = \frac{H}{c_\mathrm{p}} \tag{5}$$

$$H_\mathrm{a} = y\left(\frac{dT}{dy}\right)_S = y\frac{\alpha \boldsymbol{g} T}{c_\mathrm{p}} \tag{6}$$

Where H is the internal radiogenic heat production, α is the thermal expansivity, c_p is the heat capacity, and the other parameters are as defined earlier. We do not embed secular cooling and H_r remains constant to keep the models in the same regime throughout their evolution. We use a free-slip boundary condition on all the model space walls.

The melt fraction F (T, p) is evaluated as a function of the super-solidus temperature and pressure, following McKenzie and Bickle (1988) and using the parameterized solidus of Katz et al. (2003). The dimensionless super-solidus temperature is defined as:

$$T' = \frac{T - (T_\mathrm{sol} - T_\mathrm{liq})/2}{T_\mathrm{liq} - T_\mathrm{sol}} \tag{7}$$

we then calculate the melt fraction F as:

$$F = a + T' + (T'^2 - b)\,(c + d\,T') \quad (8)$$

with a = 0.5, b = 0.25, c = 0.4256 and d = 2.988 (McKenzie and Bickle, 1988). Here, the melt is considered extracted from the model, that is it is not added to the overlying crust (e.g., van Thienen et al., 2004), leaving a residue that is depleted by a melt fraction F, henceforth the depletion degree. In this work we do not model the sub-solidus adiabatic decompression path: adiabatic cooling reduces melting rates by ~10 %, as energy is converted into adiabatic expansion, rather than melting (Phipps-Morgan, 1997). Because we focus on the role depletion has on the residue, we do not model the latent heat due to melting. Therefore, the estimates of volumes and melting-degree represent an upper bound.

All materials' densities have the same linearized equation of state accounting for the density decrease due to depletion fraction F:

$$\rho(T, F) = \rho_0\,(1 - \alpha\,T + F\,\frac{\delta\rho_F}{\rho_0}) \quad (9)$$

where ρ_0 is the reference density and $\delta\rho_F$ the change in density due to depletion. This latter property is estimated to vary linearly by 0.726 kg m^{-3} per depletion percent (Schutt and Lesher, 2006), whence $\delta\rho_F$ = –72.6 kg m^{-3}. The value chosen here follows previous geodynamic studies (e.g., Ito et al., 1999; van Hunen and Moyen, 2012).

2.2. Constitutive laws

We use linear visco-plastic rheologies focusing on the non-linear effect of temperature following Rolf et al. (2018) and Rozel et al. (2017):

$$\eta(T) = A\,\eta_0 \exp\left(\frac{E_a}{R T_\mathrm{P}}\right) \quad (10)$$

where η is the viscosity, A is an adimensional pre-factor, η_0 is the reference viscosity, E_a is the activation energy, R the gas constant and T_P the potential temperature (Table 1). Following these works, the activation energy is E_a = 200 KJ mol^{-1}, for computational stability. Although this is lower than laboratory constrained activation energies, it results in strong thermal viscosity variations, which have been tested extensively in the referenced works.

Dehydration stiffening follows the melt-depletion of the mantle forming mineral olivine (Hirth and Kohlstedt, 1996; Mei and Kohlstedt, 2000). An empirical law commonly used to express melt-dependent viscosity is of the form $\eta(F) \sim (1 - F)\exp(\theta F)$ (e.g., Dunnberg and

Heister, 2016), where the first term in the r.h.s. expresses the volume fraction and the second the viscosity change, with θ a constant. This equation captures the viscosity drop as melt is produced, while the viscosity of the residue increases, as melt is extracted (Kohlstedt and Hansen, 2015). Here, we use this equation for the residual viscosity increase, modified to account for the solid-liquid viscosity ratio increase, best expressed by a non-linear function of the melt fraction, the Einstein-Roscoe equation:

$$\eta(F,T) = A\,\eta^{*} \exp\left(\frac{E_a}{RT_{\mathrm{P}}}\right)\left(1-\frac{F}{F_{\max}}\right)^{-2.5} \exp\left(\theta F\right) \qquad (11)$$

With η^{*} a reference viscosity, see below) and $1/F_{\max}$ = 1.35 [see (Kohlstedt and Hansen, 2015; Pinkerton and Stevenson, 1992) and references therein].

The dehydration stiffening has three main features (Hirth and Kohlstedt, 1996): *i*) negligible (~10-fold) viscosity increases between the wet and the dry solidi, *ii*) a sharp viscosity jump of a factor ~100 across the wet-to-dry solidus transition, and *iii*) a further increase of ~3-4 times per 10 % depletion. Differences between batch and fractional melting are negligible. We follow Ito et al., 1998, and Phipps Morgan, 1997, and model the 100-fold and following milder increase in viscosity. These features are captured by eq. (11). The viscosity increases in the wet and dry melt-depletion, ~3-4 times per 10 % depletion, using θ = 5.7, whereas we use $\eta^{*} = \eta_0$, for the wet domain, and $\eta^{*} = \eta_0^{\mathrm{dry}} = 40\,\eta_0$ for the melting in the dry domain (e.g., Ito et al., 1999). The transition between domains is modelled with the same exponential function of F, with θ = 47.7 (Fig. 1, B, thin solid line labelled $\eta^{\text{wet-to-dry}}$), to yield a 100-fold increase at F = 0.1. The constitutive laws are then combined using a harmonic mean (Fig. 1, B, pink line). The initial stiffening achieved below the wet-to-dry transition is neglected following the published approaches. Several numerical tests show that the increase in viscosity and buoyancy in the wet domain is not sufficient to resist mantle flow, and that the residue is remobilized in convection and does not contribute to the lithosphere strength.

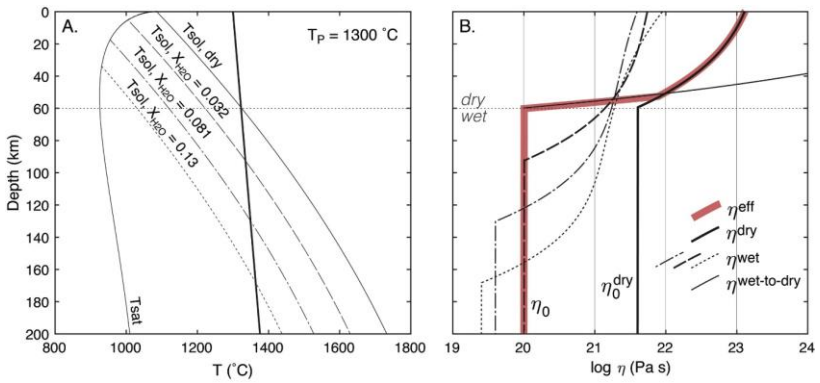

Figure 1. Mantle adiabats for present-day mantle potential temperatures at a mid-oceanic ridge and viscosity for different water contents, versus depth. (A) potential temperatures for the present day and solidi for dry, wet (with variable water content) and water saturated mantle, from (Hirth and Kohlstedt, 1996). (B) viscosities of wet (dashed lines), dry (solid thick line) and wet-to-dry transition (thin black line). In pink, the effective viscosity used in this study. Viscosities are calculated using a background strain rate $\dot{\epsilon} = 10^{-15}$ s^{-1}.

The use of Lagrangian particles allows separation of the crust and mantle materials, and we implement differentiated plasticity laws to reproduce the rheological layering of the lithosphere. For the mantle, we implement a pseudo-plastic flow law using a Drucker-Prager-type yield criterion:

$$\sigma_Y = \sigma_0 + p \sin \phi \quad (12)$$

with σ_0 the cohesion stress at surface conditions and ϕ the internal friction angle.

The rheology of the crust is differentiated following a Byerlee's law for near-surface conditions, where the cohesion vanishes, $\sigma_0^C = 0$, which is averaged using a harmonic mean with the lithospheric yield stress σ_Y:

$$\sigma_Y^C = \min(p \tan \phi, \sigma_Y). \quad (13)$$

The different depth-dependent coefficients in eqs. (12) and (13) allow the crust to be weaker than the mantle at near-surface conditions.

The plastic flow law is implemented as following:

$$\eta = \min(\eta(T), \frac{\sigma_Y}{2\dot{\epsilon}_{II}}) \quad (14)$$

where σ_Y is either that of the mantle or the crust, i.e., eq. (12) or (13), and $\dot{\epsilon}_{II} = \sqrt{(\dot{\boldsymbol{\epsilon}} : \dot{\boldsymbol{\epsilon}})/2}$ is the square root of the second invariant of the strain rate tensor, defined as:

$$\dot{\boldsymbol{\epsilon}} = \frac{1}{2}[\nabla \mathbf{u} + (\nabla \mathbf{u})^T]. \quad (15)$$

The crust in the model is defined as the inflow across the non-adiabatic basal (Moho) temperature of 320 ˚C. There is no attempt to address the nature of the crust, whether basaltic or continental, here this represents only a weak layer on the top.

Symbol	**Definition**	**Value**	**Unit**
D	Height	660	km
L	Length	7920	km
$\boldsymbol{g}$	Gravitational acceleration	9.81	$m\,s^{-2}$
T	Temperature		$^\circ C$
α	Thermal expansivity	3×10^{-5}	K^{-1}
H	Heat production	$[0, 3] \times 10^{-11}$	$W\,kg^{-1}$
c_p	Heat capacity	1200	$J\,kg^{-1}K^{-1}$
κ	Diffusivity	1×10^{-6}	$m^2\,s^{-1}$
k	Conductivity	3.96	$W\,m^{-1}\,K^{-1}$
ρ_0	Reference density	3300	$kg\,m^{-3}$
η_0	Reference viscosity	1×10^{20}	$Pa\,s$
η_0^{dry}	Reference viscosity dry	$4 \times \eta_0$	$Pa\,s$
A	pre-factor	9.1963×10^{-9}	–
E_a	Activation energy	2×10^5	$J\,mol^{-1}$
R	Universal gas constant	8.314	$J\,K^{-1}\,mol^{-1}$
σ_Y	Yield stress		MPa
σ_0	Cohesion	$[1, 70]$	MPa
σ_Y^C	Crust yield stress		MPa
σ_0^C	Crust cohesion	0	MPa
ϕ	Internal friction	0.64	rad
F	Melting fraction		–
$1/F_{max}$		1.35	–
θ		5.7	–

Table 1. Symbols, definitions and values of the dimensional reference parameters used in this study.

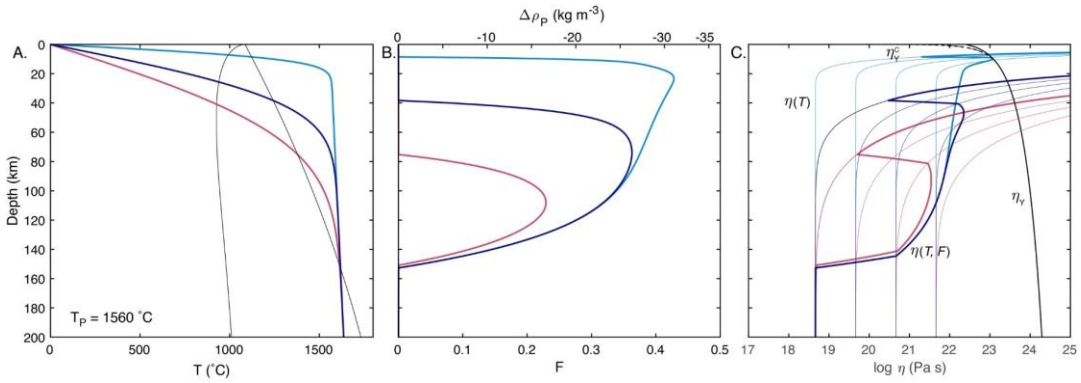

Figure 2. Selected lithospheric geotherms for different thicknesses mimicking thinning and rifting, and corresponding depletion fractions, density contrasts and viscosities, for early Earth-like mantle potential temperature T_P = 1560 ˚C, see text). (A) the geotherms (half-space cooling) reproduce the effect of thinning of the lithosphere (magenta to blue and indigo). Thin lines for the dry and water-saturated solidi. (B) the depletion degree and volumes are a function of the super-solidus temperature, and increase with thinning during rifting, becoming increasingly shallow. The potential density change is shown on the same plot as $\Delta\rho_P = F\,\delta\rho$. (C) The depletion-dependent viscosity during rifting increases with thinning, as larger melting is produced and embedded in the lithosphere. Thin lines are viscosities for η_0, 10 η_0, 10^2 η_0 and 10^3 η_0 for the temperature-dependent viscosity $\eta(T)$ and temperature- and depletion-dependent viscosity $\eta(T, F)$. Plastic viscosities are η_Y for the lithospheric yielding and η_Y^C for the crust. The viscosity is calculated using σ_0 = 50 MPa for the lithosphere and background strain rate $\dot{\epsilon}_0 = 10^{-15}$ s^{-1}.

2.3. Model setup and modelling parameters

We model convection in the upper mantle in a space of 660 × 7920 km, discretized in 64 × 768 elements, embedding a total of 983040 Lagrangian particles. We have run a total of 31 models, varying values of internal heat production H, and cohesion stress σ_0 (Table 2). Internal heat production through time is constrained by the decay of radiogenic heat producing elements *U*, *Th* and *K* in the Earth mantle (Turcotte and Schubert, 1982). Over the Earth's age of ~4.5 Ga, this varies exponentially between present-day values of $H = 3 - 7 \times 10^{-12}$ W kg^{-1} (Jaupart et al., 2015) to values in excess of 3×10^{-11} W kg^{-1}, in the Hadean, for a bulk silicate Earth (BSE) (Turcotte and Schubert, 1982). We cover this range running models with H = 0, 1, 2 and 3×10^{-11} W kg^{-1} (Table 2). The models run for a total time of 1 billion years (Gyr). The internal heat

297 production and the basal temperature are constant in the model run (Table 1), that is we do not
298 reproduce the decaying radiogenic heat nor secular cooling. Although the half-life of radiogenic
299 elements is in this order, ~1-1.25 Gyr, the choice of constant internal heat production follows the
300 idea that the convection models do not attain steady state (Korenaga, 2017). Therefore, we run
301 them for long enough to exclude any control of the radioactive decay. The values of the cohesion
302 are varied between σ_0 = 70 and 1 MPa (Table 2), covering the range from laboratory-constrained
303 values for pristine rocks to those reduced by pore pressure (Gerya, 2009).
304 The models start from a common initial configuration. This is achieved running a model
305 of convection for 500 Myr with a Rayleigh number $Ra = 10^7$, no melting and a basal temperature
306 of T = 1750 ˚C, T_P = 1430 ˚C, while at the top T = 0 (Fig. 3).
307
308
309

Model	H ($\times 10^{-11}$ W kg^{-1})	σ_0 (MPa)
1	0	10
2	0	20
3	0	30
4	0	40
4	0	50
5	0	60
6	1	1
7	1	5
8	1	7
9	1	10
10	1	20
11	1	50
12	2	1
13	2	5
14	2	8
15	2	9
16	2	10
17	2	20
18	2	30
19	2	50
20	3	1
21	3	5
22	3	6
23	3	7
24	3	8
25	3	9
26	3	10
27	3	20
28	3	30
29	3	40
30	3	50
31	3	70

Table 2. List of the models runs and modelling parameters.

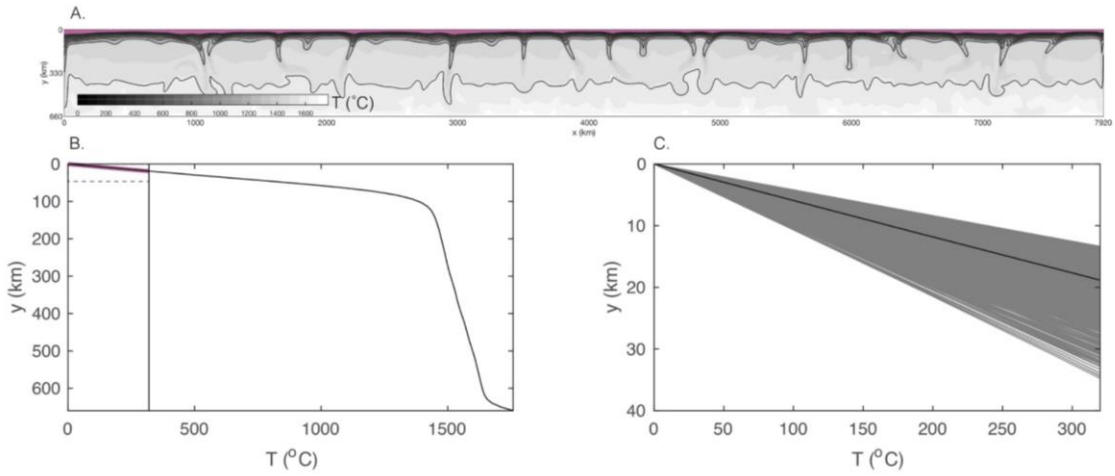

Figure 3. A. Initial temperature distribution, taken from a model under convection for 500 Myr at $Ra = 10^7$ and same rheology as in the text, but no melting. The crust is highlighted in magenta. B. Horizontally averaged temperature. The "crust" (magenta) is defined by an isotherm (vertical line, see section 4) chosen to yield a mean thickness of 20 km. Dashed line represents the box in next panel. C. All model geotherms in grey and mean geotherm in black. The plot size is shown in previous panel and lies between dashed horizontal line and solid vertical line. The crustal thickness in the initial condition varies between ~14 and ~35 km.

3. Results

Results are presented in two groups: one for internal heat production $H \leq 1 \times 10^{-11}$ W kg^{-1}, generally corresponding to Phanerozoic values, and one for larger values tested, $H \geq 2 \times 10^{-11}$ W kg^{-1}, which correspond to inferred Precambrian values. Within these groups, models' evolution is dependent on the lithospheric strength, only.

To compare the models we use the domain-averaged mantle temperature $\bar{T}$, the potential temperature T_P, the heat flow q at surface and the surface-averaged value $\bar{q}$, the root-mean-square (rms) velocity at surface $u_{\text{rms}}^{\text{surf}}$, the surface mobility $M = u_{\text{rms}}^{\text{surf}} / u_{\text{rms}}$ and the total melt volume (area) in the top 250 km of the model $V = \int_0^{\text{L}} \int_0^{250\text{ km}} F(x,y)\, dx\, dy$, with L the width of the model space (Table 1).

To characterise the thermal evolution, we use the non-dimensional internal Rayleigh and the Nusselt numbers defined as:

$$Ra = \frac{\alpha g \rho_0 \bar{T} D^3}{\kappa\, \eta(\bar{T})}, \qquad (16)$$

$$Nu = \frac{\bar{q}D}{k\,T} \quad (17)$$

where $\eta(\bar{T})$ is the internal viscosity and kT/D is the flow in the hypothetical case of heat released by conduction only through the mantle thickness D.

3.1. Regimes with Phanerozoic internal heat production

The evolution of models with $H \leq 1 \times 10^{-11}$ W kg^{-1} reproduces those presented elsewhere (e.g., Lenardic, 2018), ranging from a poor surface mobility, to a rather mobile lid, with characteristics of present-day plate tectonics. These regimes onset rapidly and remain with similar features throughout the model run.

The models with high cohesion, $\sigma_0 \geq 20$ MPa, develops a continuous lid above the convective mantle with limited mobility. The mantle viscosity in these models is ~10^{20} Pa s, while the lithosphere attains similar viscosities in these models, being thermally activated, and limited by the yield strength of the lid, and negligible depletion occurs. We show the model with cohesion 20 MPa (Fig. 4A), where velocities remain < 1 cm yr^{-1} in the model domain. The lid develops thick down-wellings under the tractions of the convecting mantle, where crust and lithosphere are shortened. Between these, large areas of very thinned lithosphere and crust (in grey) develop. The slow stretching of the thermal boundary is counter-balanced by cooling, so that the lid does not yield. This is shown by low surface heat flow of < 40 mW m^{-2} measured above down-wellings, and larger values, yet < 100 mW m^{-2}, above stretching domains. The temperatures in these models remain consistently below the solidus, and no melting forms in the models. The potential mantle temperature decrease (Fig. 5A) at rather constant rates of ~100 ˚C/Gyr, attaining values of T_P = ~1300 ˚C by the end of the model run. The averaged heat flow rapidly reaches values $\bar{q}$ < 40 mW m^{-2} within ~300 Myr, then remaining constant throughout the model run (Fig. 5B) showing the growth of the conductive lid. Surface rms velocities remain negligible throughout the evolution of the model (Fig. 5C) with mobility M < 0.5. Similar results are found for $\sigma_0 \geq 20$ MPa, although the evolution is increasingly slower. For its reduced mobility, this regime is comparable to the sluggish lid (henceforth SL), as proposed by several workers (see Lenardic, 2018).

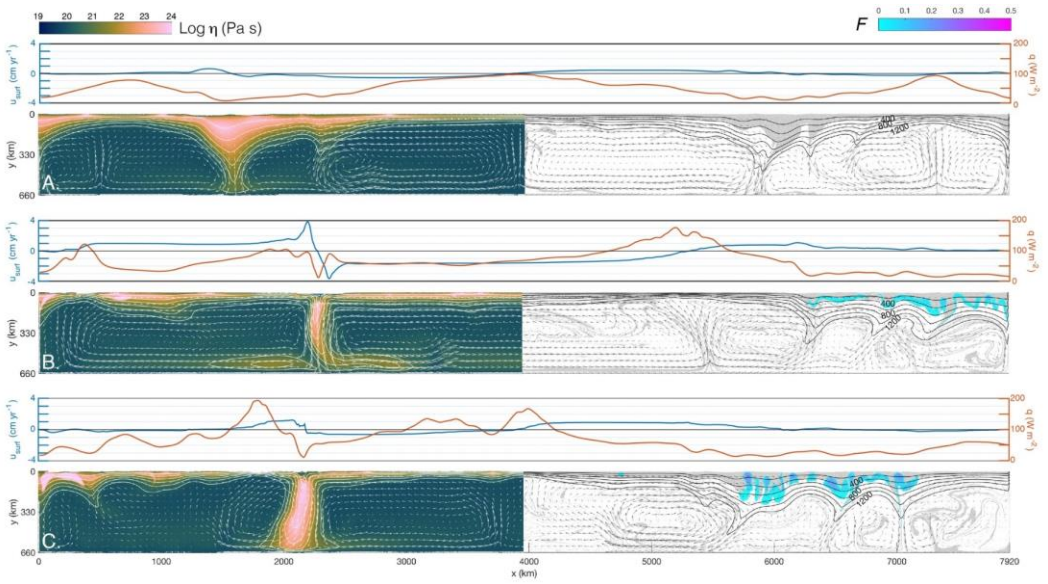

Figure 4. Models with internal heating $H = 1 \times 10^{-11}$ W kg^{-1} and varying cohesion. Cohesion is 20, 10 and 5 MPa (A, B, and C, respectively). Surface heat flow (orange) and velocity (blue), in colour-scale pink-to-blue (Crameri, 2018) viscosity and blue-magenta for depletion degree F, crust in grey in the right-hand side panels, arrows for velocity field. Temperature contours every 200 ˚C plotted for $T \leq 1300$ ˚C.

Lower mantle cohesion of $\sigma_0 = 10$ MPa allows for the yielding of the lid and its increased mobility. This regime includes divergent and convergent margins with formation and recycling of lithosphere, akin to mid-ocean ridges and subduction zones, respectively (Fig. 4B). The surface velocities in this model are larger than the previous model, with plate-like rigid broad lithospheres converging at 3-4 cm yr^{-1}. Elsewhere, thickening occurs above a down-welling, at low surface velocities < 1 cm yr^{-1}. Lower yield strength results in larger thinning, melting and depletion, although degrees remain $F < 0.1$ (Fig. 4B), and are partly preserved in the thickened down-welling, due to its buoyancy. Heat flow varies largely between ~180 mW m^{-2}, above thinned divergent centres, to very low values of <10 mW m^{-2}, in the down-welling areas, reflecting the differences of thermal boundary thickness above the convecting mantle. The evolution of the averaged mantle temperatures in this model are similar to the previous (Fig. 5A), in spite of the lid involvement in the convection and enhanced cooling. Therefore, viscosities are comparable, although lowered yielding limits the lid's maximum viscosity. Averaged heat flow

decreases initially to then increase from 250 to 600 Myrs to values in excess of ~70-80 mW m^{-2}. After this period the model's heat flow periodically varies between ~57 and ~62 mW m^{-2} (Fig. 5B), reflecting episodes of lithospheric recycling. Surface rms velocities reach values in excess of ~10 cm yr^{-1}, between 250 and 600 Myrs (Fig. 5C), then episodically increasing to comparable values. The mobility in this model is consistently large, with values between ~1 and 1.5, throughout its evolution, showing the coupled lithosphere-mantle participation in the convection (Fig. 5D). Minor melt volumes are produced throughout the model run (Fig. 5E). This regime is comparable to a mobile lid (ML) proposed in previous works [see (Lenardic, 2018).

Models with lower yield strength $\sigma_0 \leq 5$ MPa develop a similar regime to the previous models, although the lowered strength of the mantle results in a less stable lithosphere, with faster periodic recycling and subduction-like down-wellings and an overall earlier regime onset. The lowered yielding effectively fragments the lid, forming narrower plate-like blocks (Fig. 4C), while mobility remains focused at convergent zones, at rates < 1-2 cm yr^{-1}. Similar to the previous model, a thick lid forms above down-wellings, with minor depletion, which remains < 0.1 (Fig. 4C). The averaged mantle temperatures follow the same evolution of previous models (Fig. 5A), and the averaged heat flow has a rapid increase to values in excess of ~80 mW m^{-2} then decreasing to values of ~60-50 mW m^{-2} (Fig. 5B), showing effective heat extraction from the mantle. In this early stage, surface rms velocities are as high as ~15 cm yr^{-1}, then decreasing to values comparable to the previous model (Fig. 5C). The mobility in this model is consistently M = ~1 ± 0.25, showing the coupled overturn of lithosphere and mantle. Melt is mostly produced in the early stage of the model run, <~150 Myrs, however it then decreases, due to slow recycling of primordial depleted lithosphere (Fig. 5D). These models share similar characteristics of the mobile lid (ML) regime.

Summing up, the regimes under low internal heat production are mostly sensitive to the mantle temperature achieved and the yield strength of the lithosphere, and vary from a poorly mobile, sluggish lid (SL) to a highly mobile lid (ML). These regimes achieve a statistical steady-state rapidly, with minor melt production.

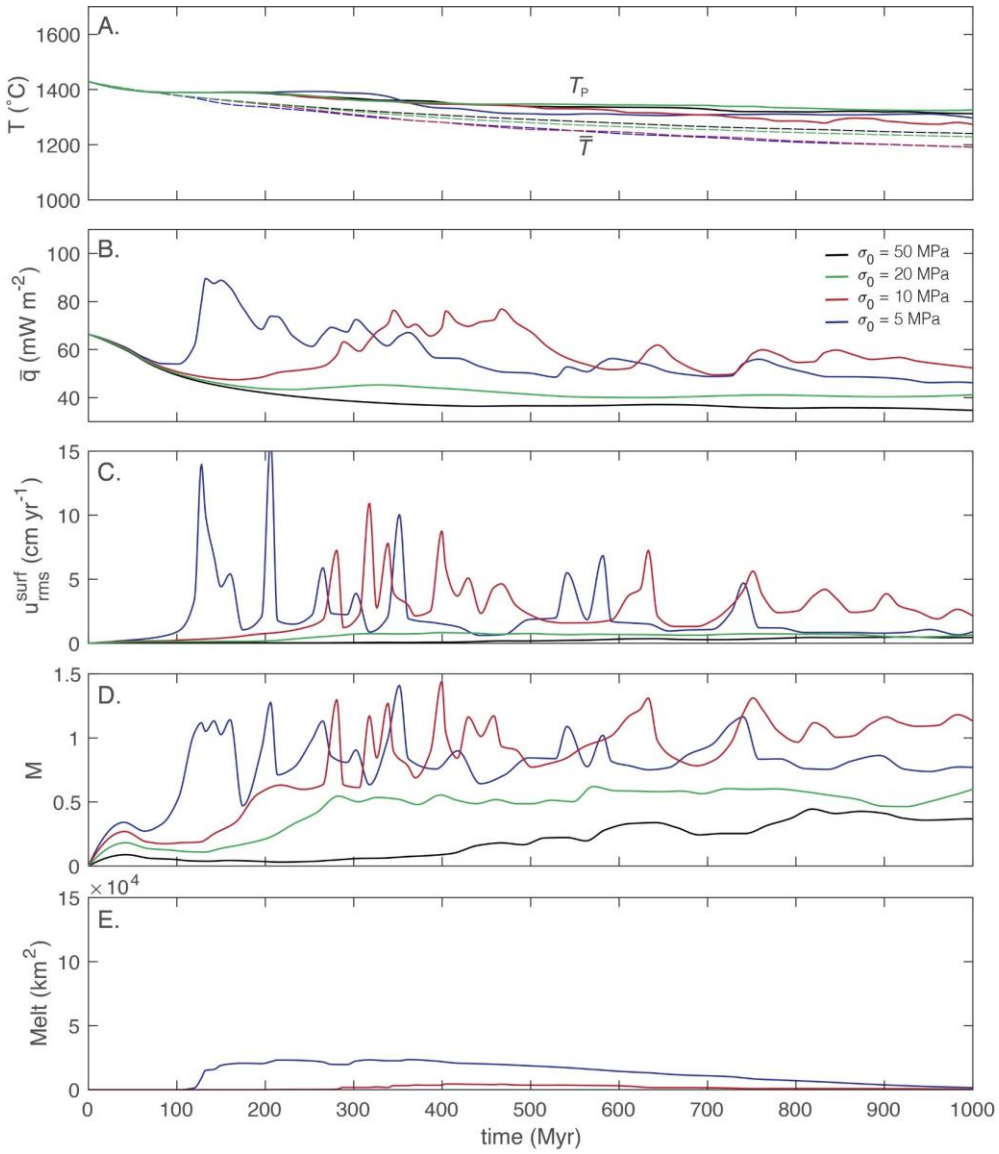

Figure 5. Models with internal heating $H = 1 \times 10^{-11}$ W kg^{-1} and varying cohesion versus time. (A) Maximum potential temperature (solid) and volume-averaged temperature (dashed), (B) surface-averaged heat flux, (C) rms surface velocity, (D) mobility and (E) melt production.

3.2. *Regimes with Precambrian internal heat production*

With increased internal heat production, $H \geq 2 \times 10^{-11}$ W kg^{-1}, higher mantle temperatures are achieved, resulting in large volumes and degrees of melt depletion, and the progressive thermochemical differentiation of the upper mantle into a stiffer lithosphere. These models have

very different and time-dependent evolutions: under conditions favourable to a mobile lid regime, that is low yield strengths, larger melting, heat extraction and dehydration stiffening opposes mobility, tending to stabilise the lithosphere and suppressing the formation of margins. Within this regime, a mobile lid evolves in a rather thick, stagnant lid, as mobility vanishes, therefore we call this regime *lid-and-plate* (LP), following Capitanio et al., 2019. Instead, with high yield strength, models develop a sluggish lid which evolves towards a stagnant lid, as minor volumes of melting form, and we call this regime *sluggish-to-stagnant lid* (SSL). The mantle differentiation and stabilisation of the lithosphere suppress any episodicity, and the evolution towards a thermochemical lid is irreversible.

In models with high mantle cohesion tested, $\sigma_0 \geq 30$ MPa, small depletion degree is achieved under a sluggish lid, evolving into a stagnant lithosphere. The lid develops down-wellings while the stretching lithosphere in between progressively thins. Below areas of thinned lithosphere and crust, melting occurs and stiffer, depleted blocks of lithosphere form in the area where melting occurs. These are continuously formed beneath a stretching lid, with low depletion degree, ~0.2, episodically reaching ~0.35 (6, A, right panel). As progressive stiffening inhibits further stretching, the strain migrates laterally, allowing cooling and embedding of depleted mantle blocks in the lithospheric mantle (Capitanio et al., 2020). These remain preserved as high viscosity (6, A, left panel), depleted blocks (6, A, right panel). The progressive formation of residual lithospheric mantle blocks stabilises the lid, and transforms it into a stagnant and almost uniformly thick lid. Lowered viscosity of a hotter mantle favour small drips beneath the rigid lid, while down-wellings of large volumes are suppressed. Velocities remain < 0.5 cm yr^{-1} everywhere in the model by the end on the run (Fig. 6A), and a rather constant surface heat flow of ~30 to 80 mW m^{-2} is observed, reflecting the small variations in lid thickness. The mantle temperature in these models increases, due to the internal heat generation and the progressive lid stiffening, while the mantle viscosity decreases to values ~10^{19} Pa s. Potential mantle temperatures increase with the large internal heating (Fig. 7A) at rather constant rates of ~200 ˚C/Gyr, reaching values T_P > 1600 ˚C. This regime stabilises rapidly and averaged heat reaches values $\bar{q}$ = ~50 mW m^{-2} within < 200 Myr, then remaining constant (Fig. 7B), as the conductive boundary layer grows and stabilises. Surface rms velocities remain negligible throughout the evolution of the model with mobility M < 0.25 (Fig. 7C, D), suggesting a rather stable lithosphere above the vigorous convection of a hotter mantle. Melt is produced at very

small rates throughout the simulation and reach larger volumes towards the end of the simulation (Fig. 7E). These models develop a stagnant, thick lid within a regime favourable to a sluggish lid, and we call it sluggish-to-stagnant lid regime (SSL).

The models with mantle cohesion of $\sigma_0 \leq 20$ MPa develops larger amounts of depleted, stiffer lithosphere and although in the mobile lid domain, they follow a different evolution. We show in figure 6 models with cohesions of 10 and 5 MPa, which are similar. By the end of the model runs, the velocities are everywhere < 0.5 cm yr^{-1}, with minor convergence at ~0.3 cm yr^{-1} (Fig. 6B and C) and a rather uniformly thick and rigid lid has formed. These models develop large amounts of melting beneath the deforming lid, due to the larger mantle temperatures. In the models, depletion is ~0.36 almost everywhere in the domain, and ~0.45, for the two values shown, respectively. Because these models have the same strength of the mobile lid regime, similar features are formed, such as rifting and subduction-like down-wellings. However, these features are resisted and halted becoming embedded as remnants in the lithosphere, as shown in the end of the model run (Fig. 6B and C, right panel). The stabilisation of the lid is reflected by rather comparable heat flow values on the surface, with less variation, between ~30 and 60 mW m^{-2}. The increase in the lid's viscosity and the decrease in the hotter mantle prevents the formation of down-wellings. However, the lower strength allows for lid's plastic failure and the rapid recycling in the mantle (Fig. 6B). Mantle temperatures increase as in the previous models (Fig. 7A), while the other parameters best illustrate the evolution of this regime. These models, with cohesion ≤ 20 MPa, are in the domain of the mobile lid, and develop similar features, such as rift and subduction-like down-welling, in a first stage. These favour the emplacement of depleted, stiffer mantle, which acts to suppress them. This negative feedback progressively hampers mobility, until the lithosphere is stabilised. The averaged heat flow shows an initial stage of large heat release (Fig. 7B), which varies according the cohesion value between ~100 and 550 Myrs, then achieving a rather stable value of ~50 mW m^{-2} in the second stage. This reflects the initial rapid overturn and recycling similar to the ML (Fig. 4B) and high surface rms velocities up to ~15 cm yr^{-1}, sustained for short periods of ~150 Mrs (Fig. 7C, D). In this early stage, the mobility is consistently M = 1 to 1.5, then dropping in the second stage, when all the models have stabilised. It is important to note that in these models, the heat flux and velocities, although displaying similar trends, are consistently larger than in the models with lower internal heat, in this phase. While some domains develop thick low-heat flux domains, other

undifferentiated domains are forced into greater heat release by increased mobility (e.g., Lenardic, 2018).

In the second stage, from ~550 – 1000 Myrs, the mobility of the lid is reduced as a consequence of the pervasive depletion and stiffer lithosphere volumes. The melt evolution shows that most of the volume is produced in the first phase (Fig. 7E). This implies major stiffening, which suppresses mobility and the plate tectonics-like features, while preserving them as remnant fossil features. In this stage, all these models attain similar heat flow of ~50 mW m^{-2}, surface velocities <~4 cm yr^{-1}, and mobility as low as ~0.5. Lithosphere recycling occurs, although less frequently and along shortly lived subduction-like down-wellings, where minor amount of melt is extracted and lithosphere and crust are recycled. These episodes occur until the end of the model run showing that the lid stabilises, yet allows for continuous, albeit minor, recycling.

These models show an evolution in two stages: an initial stage with a mobile lithosphere and plate margin-like features, and a second stage when the thermochemical differentiation suppresses mobility and turns the lithosphere into a stagnant lid, embedding early stage fossil tectonics features. Large melting and recycling are features of the early stage, while minor melting and recycling occur in the second stage. At no stage do the models show complete overturn (e.g., O'Neill et al., 2007), and features formed throughout the evolution are preserved.

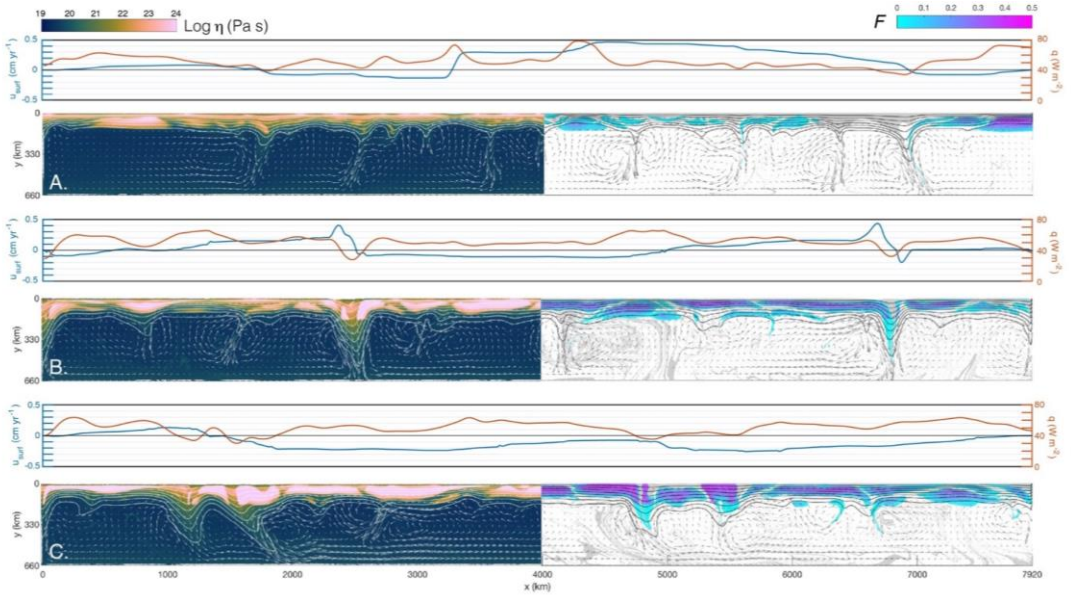

Figure 6. Models with internal heating $H = 3 \times 10^{-11}$ W kg^{-1} and varying cohesion. Cohesion is 20, 10 and 5 MPa (A, B, and C, respectively). Surface heat flow (orange) and velocity (blue), in colour-scale pink-to-blue viscosity and blue-magenta for depletion degree F, arrows for velocity field. Temperature contours every 200 ˚C plotted for $T \leq 1300$ ˚C.

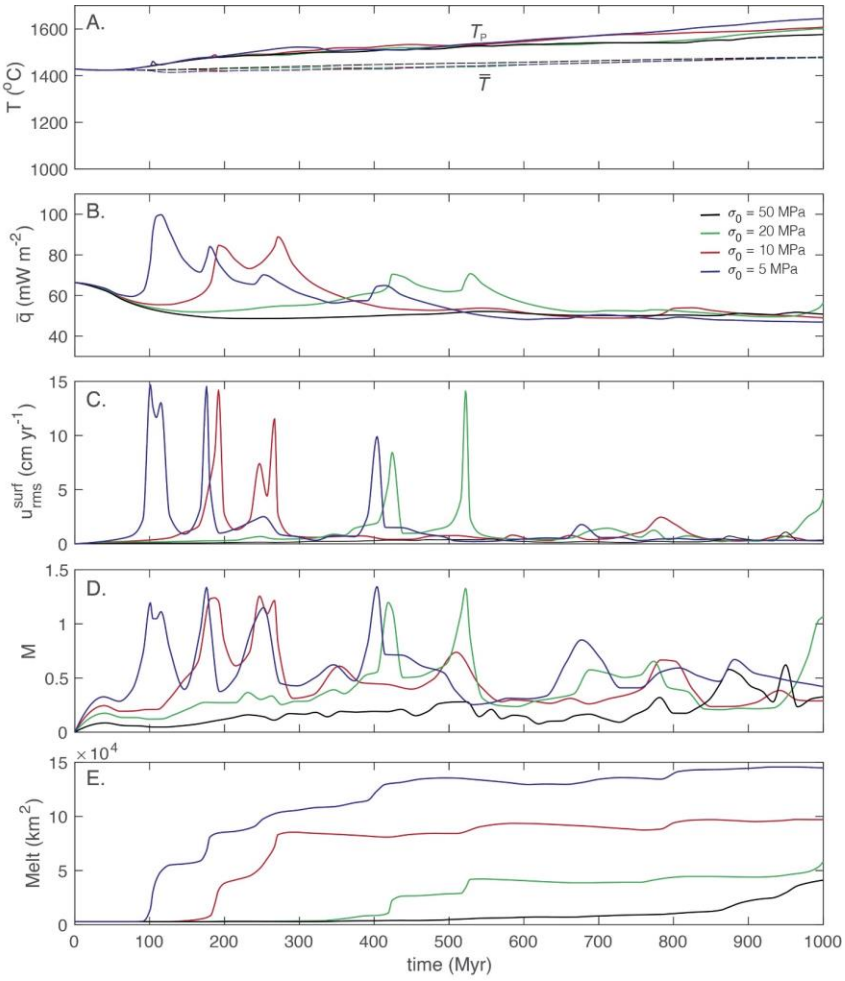

Figure 7. Models with internal heating $H = 3 \times 10^{-11}$ W kg^{-1} and varying cohesion versus time. (A) Maximum potential temperature (solid) and volume-averaged temperature (dashed), (B) surface-averaged heat flux, (C) rms surface velocity, (D) mobility and (E) melt production.

3.3. Internal heat and yield strength controls on the tectonic regimes

The controls of thermochemical differentiation on tectonic regimes are best illustrated in the internal heat production–yield strength parameter space, following O'Neill et al., 2007.

The models with Phanerozoic internal heat production $H \leq 1 \times 10^{-11}$ W kg^{-1} develop regimes that are dependent on the lithospheric strength (Fig. 8). For strengths $\sigma_0 \geq 20$ MPa, the lithosphere undergoes stretching, allowing for little mobility in the SL regime, although no margins form. For strengths $\sigma_0 \leq 10$ MPa the models are in a ML regime, with mobility $M > 0.8$ and increasingly episodic behaviour with decreasing strength.

Mantle potential temperatures tend to similar values for a constant internal heat production, in spite of different yield strength. Therefore, depletion remains controlled by yielding, allowing for the thinning of the lid and the shallowing of the geotherm above the solidus, favouring larger melting volumes and degrees. In these models, maximum depletion degrees reach 0.05 to 0.1 in the ML regimes, whereas no melting occurs in the SL regime. The small volumes and degrees of depleted lithosphere formed do not reduce the mobility of the lid.

For Precambrian internal heat, $H \geq 2 \times 10^{-11}$ W kg^{-1}, higher melt-depletion stiffening hampers the lid mobility of the ML and SL regimes, forcing a time dependent evolution. In models with higher strengths, depletion degrees increase with internal heating (Fig. 8). In models with yield strength >10-20 MPa, favourable to SL, the lithosphere transitions to a rather stagnant lid (SSL). This occurs for models with maximum F = ~0.1 to ~0.3, when the dehydration stiffening is large enough to prevent the sluggish motions. For strengths tested above 50 MPa, lithospheric thinning tends to vanish, no thermochemical differentiation occurs, in spite of the high temperatures, and the models remain in the SL domain throughout their evolution.

Towards the lower strength end, in a field equivalent to the ML regime, large depletion forces transition to the time-dependent regime LP, below critical yield strength 10 to 20 MPa. In the LP regime the maximum depletion degree is constantly >~0.3. and reaches values >0.4 (Fig. 8). However, for decreasing strength, <5 MPa, the lithosphere becomes increasingly unstable, and the increasing melt production is associated with increasing lithosphere recycling.

The conditions for the SL and ML regimes are less dependent on H for Phanerozoic values, however, when thermochemical differentiation is considered, the boundary between low and high strength regimes, LP and SSL, has a positive slope increasing with internal temperatures and H. This is likely related to strength heterogeneities due to residual stiffer bodies in the lithosphere which favour stress localisation and yielding of a stronger sluggish lid. The

role of thermochemical differentiation is further emphasised by the alignment of the boundary between low and high temperature/internal heat regimes with the depletion contours, although here are not constrained further. This boundary is likely narrow, because of the threshold nature of the plastic rheology. The lithospheric strengthening increases with volumes and depletion degrees; while for small volumes/degrees this has a minor impact on the lithospheric strength, and is recycled, when strengthening grows above the lithospheric stress, the lid stabilises. Here, we illustrate this process but do not constrain the critical depletion degree at which the boundary between these field is located. In fact, this remains dependent on the parameter chosen here, nevertheless it illustrates ideal scenarios for the Earth.

These regimes show that the role of lithospheric yield strength under Precambrian conditions is minor and depletion is major, compared the opposite roles these have in the Phanerozoic-like radiogenic heat models. As a consequence, models with different yield strengths tend to evolve in a similar way. Additionally, the lid stabilisation suppresses periodic recycling. Models with strength above realistic values are insensitive to internal heat production.

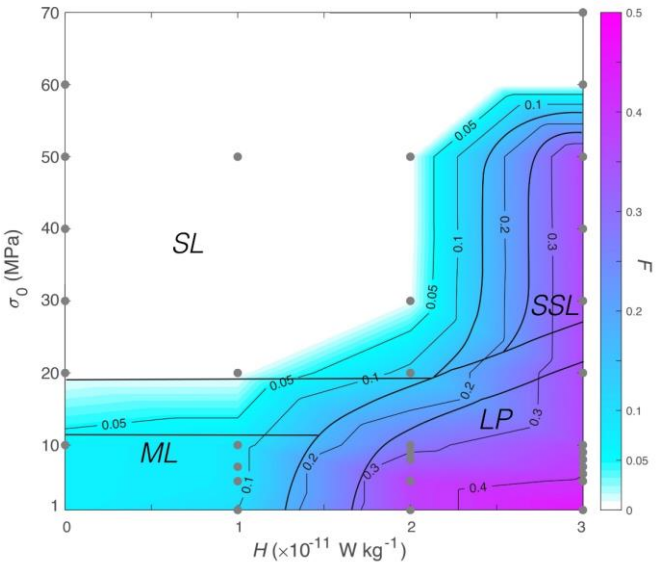

Figure 8. Regime diagram of models with varying internal heating and cohesion. In colour scale the maximum depletion degree in the model F. The regimes are sluggish lid (SL), sluggish-to-stagnant lid (SSL) for large yield strength, and mobile lid (ML) and lid-and-plate (LP) for lower yield strength.

3.4. Thermal evolution

The thermal evolution of the models can be tested against "classical" parameterised convection scaling (e.g., Davies, 1980). In this approach, the balance between internal heat and heat released through the surface is captured by the power-law:

$$Nu \sim Ra^{\beta}, \quad (18)$$

where the exponent β expresses the sensitivity of surface heat flux (*Nu*) to the vigour of convection (*Ra*), that is internal temperatures and viscosity.

The value of β for these regimes varies. Thermal boundary layer theory for isoviscous convection finds β ~1/3 and 1/4 for basally and internally heated fluid with free-surface boundary conditions, respectively (Turcotte and Oxburgh, 1967). Numerical modelling and scaling analysis extend this finding to cases with temperature- and stress-dependent rheologies, forming stagnant to mobile lid, plate tectonics-like, regimes (Moresi and Solomatov, 1998). At high viscosity contrast and large bending dissipation decreases to $\beta < 0.1$ or ~0, showing the lid's independence on convection (Christensen, 1985; Conrad and Hager, 1999). For the early Earth, a weaker heat release dependence on internal temperature must be invoked (Davies, 1980) and Korenaga (2003) proposed a thermochemical boundary layer, that is the dehydrated, stiffer mantle layer forming by melt extraction, which thickens with increasing mantle temperature. For such case a negative heat flow-internal temperature relation is found with $\beta = -0.15$.

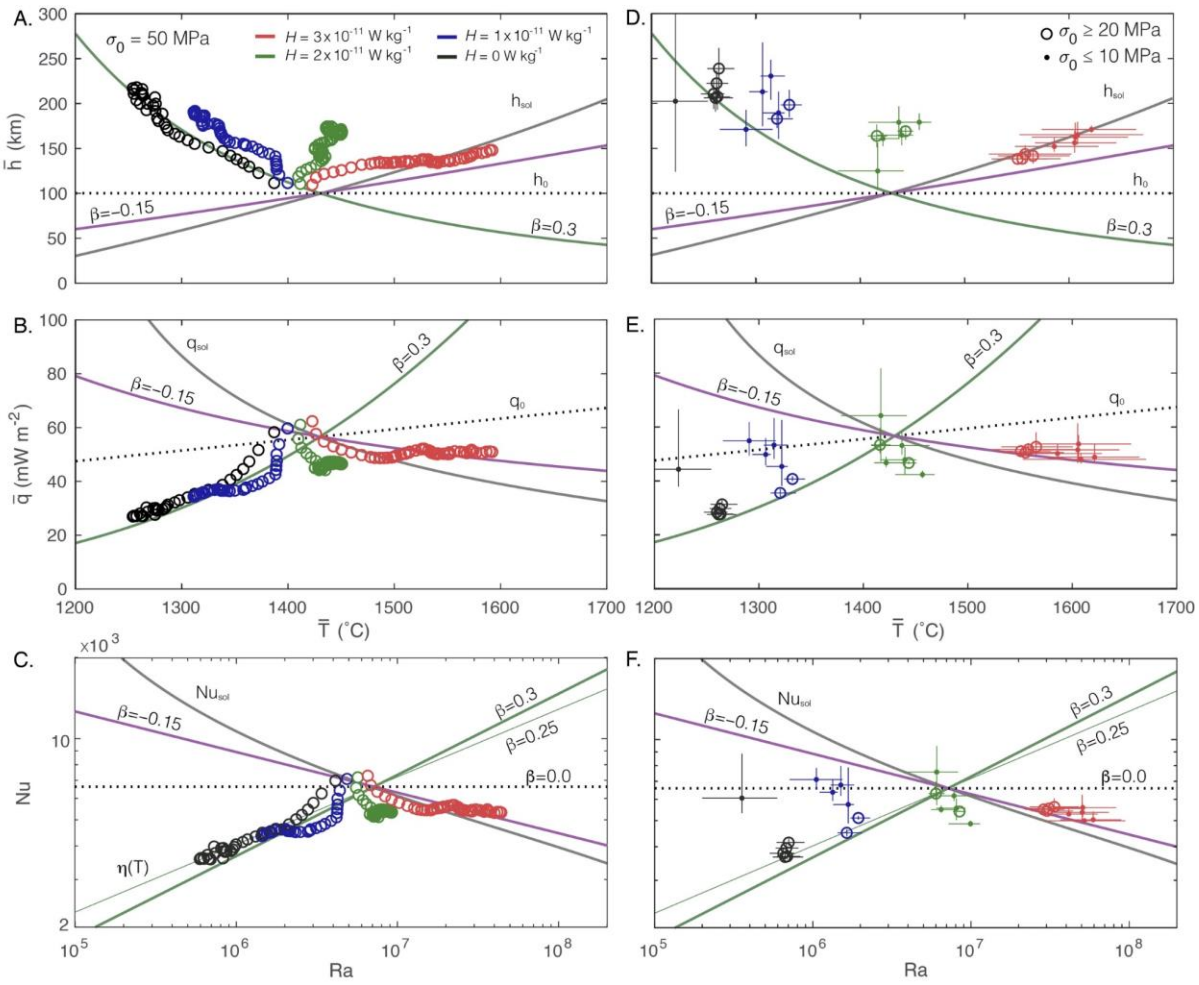

Figure 9. Lithosphere average thickness, surface heat flow versus internal averaged temperature and Nusselt vs. Rayleigh number of the models. (A to C) evolution of models with high yield strength, σ_0 = 50 MPa, and varying internal heat, every 50 Myr. (D to F) values from all models, time-averaged over the last 400 Myr of the model runs. Open circles for models in SL and SSL regimes ($\sigma_0 \geq 20$ MPa) and solid dot for models in ML and LP regimes ($\sigma_0 \leq 10$ MPa). Trends for β = 0.25 and 0.3 (thin and thick green lines), β = –0.15 (purple) and values calculated with maximum depth of melting (grey lines). Dotted line for reference values, calculated with h_0 = 100 km.

We follow Davies, 1980, and from (18), combining eqs. (16) and (17), the scaling of heat flow is:

$$\bar{q} = a \frac{\bar{T}^{\beta+1}}{[\eta(\bar{T})]^{\beta}} \qquad (19)$$

603 then, the scaling for the average thickness of the boundary layer $\bar{h}$ is:

604 $$\bar{h} = b\left(\frac{\eta(\bar{T})}{\bar{T}}\right)^{\beta} \quad . \qquad (20)$$

605 Here, the parameters a and b are determined readjusting the heat loss equation to a reference heat
606 flow, thickness and temperature (e.g., Christensen, 1985):

607 $$\bar{q} = q_0 \left(\frac{\bar{T}}{T_0}\right)^{\beta+1} \left(\frac{\eta(T_0)}{\eta(\bar{T})}\right)^{\beta} \qquad (21)$$

608 $$\bar{h} = h_0 \left(\frac{\eta(\bar{T})}{\bar{T}} \frac{T_0}{\eta(T_0)}\right)^{\beta} \qquad (22)$$

609 where $q_0 = k\ T_0/h_0$, $T_0 = 1430$ ˚C, $h_0 = 10^2$ km and $\eta(T_0)$ is the internal viscosity at T_0.
610 Additionally, we define the depth of melting h_{sol}, found setting $T(y) = T_{sol}(y)$, which depends on
611 the solidus chosen here (Katz et al., 2003), and show for reference the corresponding heat flow
612 q_{sol} and Nu_{sol}. Because the models do not attain a steady state, they display, for large internal
613 heat, strongly time-dependent evolutions and deviations from mean values, compromising the
614 meaningfulness of the statistical averaging. Therefore, here we do not quantify a fit for β, but
615 rather provide a qualitative test of the scaling.

616 We first show the comparisons of models with large strength, in poorly mobile lid
617 regimes, SL and SSL. Measurements are taken every ~50 Myrs, to illustrate the models'
618 evolution (Fig. 9A-C). The thickness of the lithosphere is measured as the depth of greatest
619 geotherms' gradient, which is considered here the lithosphere-asthenosphere boundary. The
620 models in the SL regime show thicknesses and the heat flow evolving from the models' initial
621 conditions towards lower internal temperatures, yet align with the thermal boundary layer scaling
622 defined by β ~0.3 (Fig. 9A, dark green line). The models follow similar scaling for small
623 amounts of dehydration stiffening, $F < 0.1$, although the averaged lithospheric thickness is < 10
624 % larger in models with $H = 1 \times 10^{-11}$ W kg^{-1} where depletion is closer to the upper limit (Fig.
625 9A, blues circles). Instead, the model with largest internal heat tested, develops rapidly a thicker
626 lid with increasing temperature and depletion (Fig. 9A, red circles). The thickness values vary
627 between the depth of the melting h_{sol} (grey line) and that found using β = –0.15 (purple line) in
628 the scaling, following the thermochemical boundary layer scaling. For values of internal heat H =
629 2×10^{-11} W kg^{-1} the model undergoes a mixed evolution with temperature relatively constant for
630 slightly increasing thickness (Fig. 9A, green circles). In this regime, depleted volumes decrease
631 and both end-member features appear (see below). The heat flow follows closely the trend with β

~ 0.3 in models with $H \leq 1 \times 10^{-11}$ W kg^{-1} (Fig. 9B). For largest internal heat production, heat flow evolves between q_{sol} and the $\beta \sim -0.15$ trend, while the intermediate values of internal heat fall between. Similar trends are reproduced in the *Nu – Ra* scaling, although the values for lowest internal heating are best matched by a value $\beta \sim 0.25 – 0.3$ (Fig. 9C, black and blue circles). The models with value $H = 2 \times 10^{-11}$ W kg^{-1} reach rapidly intermediate values between the two trends (Fig. 9C, green circles).

Using time-averaged values in the last 400 Myr of the runs, we illustrate all the models (Fig. 9D-F), divided in the SL – SSL regimes (open circles) and in the ML – LP regimes (dots) for mean values, while the range bars indicate the deviation. All models in SL and SSL regimes tend to follow the scaling illustrated by the single models full evolution (Fig. 9, open circles). However, at lowered lid strength, the models in the ML regime (black and blue dots) deviate and heat flow tends to be less dependent of internal temperature, showing a scaling exponent β from 0.3 to 0, in which case a rather constant thickness dominates. Interestingly, at the largest internal heat tested, the models align clearly with the trend set by $\beta \sim -0.15$ (purple line), with little deviation. This shows consistently that the differentiation of the thermochemical lid has a stronger control on the thermal evolution than the thermal boundary layer, and narrows the possible regimes in the hotter Earth. Models with an intermediate internal heat, $H = 2 \times 10^{-11}$ W kg^{-1}, show an intermediate behaviour and a less time-dependent evolution, which is discussed below.

4. Discussion

4.1.Implications for long-term thermal evolution

The most important test for the viability of tectonics regimes and their evolution resides in the thermal regime they predict when extended to early Earth conditions. The heat budget of convection depends on the balance between the internal heat and its loss at surface (Turcotte and Oxburgh, 1967). This focuses on the thickness of the conductive thermal boundary layer and its relation with the internal heat. This has been approached by means of parameterised scaling (Foley, 2018), while comparisons to modelling allowed testing the role of complex lithospheric rheologies, from strong dependence on temperatures (Christensen, 1985; Davaille and Jaupart, 1993), to non-linearities and plasticity (Moresi and Solomatov, 1998; Moresi and Solomatov,

1995; Solomatov, 1995; Tackley, 1998, 2000; van Heck and Tackley, 2008), and to inherited damage (Foley and Bercovici, 2014).

In the parameterised approach, the dependence between the heat flow and the internal convection regime, i.e. $Nu \sim Ra^{\beta}$, describes the sensitivity of the former, and therefore the lid thickness, to the internal temperature. From boundary layer theory it can be derived $\beta = 1/3$ and 1/4 for basally and internally heated fluid with free-surface boundary conditions, respectively (Turcotte and Oxburgh, 1967), implying that the convection regime limits the growth of the thermal boundary layer. This scaling is confirmed by laboratory and numerical modelling, showing the co-dependence of internal heat and its release through the lid (Christensen, 1985; Davaille and Jaupart, 1993; Moresi and Solomatov, 1998). Here, albeit simplified, models with small amounts of depletion agree with these findings, suggesting a $\beta \sim 0.25$ - 0.3 for internal heat and melting comparable to present-day in the stagnant lid regime.

The extension of these finding to mobile lid regimes emphasises the role of the lithospheric effective strength at subduction zones. The models show a reduction of the dependence, with $\beta \rightarrow 0$ for low depletion degree-models, suggesting the thermal evolution is controlled by a rather constant lithospheric thickness across a range of temperatures. Similar drops to ~0 are found when large bending dissipation at subduction zones reduces the dependence on internal heat, and β can be < 0.1, to 0 (Conrad and Hager, 1999). However, large dissipation at the bending zone is ruled out by partitioning analysis in viscoelastic models, due to the release of elastic energy during unbending (Capitanio and Morra, 2012; Capitanio et al., 2009), in compressible mantle convection (Leng and Zhong, 2010) and boundary element analysis (Gerardi et al., 2019). Although we do not investigate further, here the variable decrease of β is explained by the trade-off between the slab buoyancy and resistance to bending, which readjust slab dip and curvature radius to minimise the dissipation (Capitanio and Morra, 2012; Capitanio et al., 2009; Davies, 2009). For low melting degrees/volumes shown in the models, this mechanism controls the hinge zone at convergent margins, resulting in rather constant dissipation partitioning (Capitanio et al., 2009) and effective thicknesses. In general, this emphasises the role of subduction zones low dissipation in the energy balance of mobile lid regimes and plate motions, as opposed to that of plates interiors (Buffett and Rowley, 2006; Christensen, 1985; Davies, 2009; Korenaga, 2006).

How this thermal evolution extends to the early Earth remains problematic, as it predicts excess internal heat release, the "thermal catastrophe", which is not confirmed by the observations (Christensen, 1985). The $Nu \sim Ra$ positive correlation ($\beta > 0$) implies that the convection vigour controls the conductive layer, with increasing mantle temperatures and heat flow through a thinner thermal boundary (Fig. 10, SL). When applied to long-term (backward) mantle evolution, that is with increasing internal heat, the thermal boundary layer scaling results in unrealistic high mantle temperatures at ~ 1.5 Ga (e.g., Davies, 1980). While possible, yet unlikely, solutions consider different internal heat production of our planet, other solutions have been proposed to solve this paradox by emphasising the role of the thermochemical differentiation in the lithosphere. Korenaga, 2003, 2006, proposes the controls of dehydrated, stiffer mantle in a hotter mantle, thereby resulting in increasing lid thickness with temperature, following the deepening of the geotherm intersection with the melting temperature, and the consequent decreasing of the heat flow through it. This results in a negative heat flow-internal temperature scaling, where *Nu* scales as a power $\beta = -0.15$ of the internal temperatures (*Ra*). In agreement with this body of work, we find that for larger temperatures, the deepening of melting depth favours thermochemical differentiation of the lithosphere, which breaks down the dependence on internal temperature and controls the thermal evolution. The scaling relation switches for increasing mantle temperatures in the models, from a thermal to a thermochemical boundary layer, when dehydration stiffening becomes dominant. However, although large internal heat is likely condition of the early Earth (Jaupart et al., 2015), the models suggest that the development of such a stagnant lid takes substantial time, which might become longer with a more realistic decaying internal heat, as opposed to the constant values used in the models. Within the early phase, <500 Myr, stretching and differentiation localise, and therefore the lid develops domains with low heat flux, akin to continents, and domains with large mobility and less differentiation, where the heat flux can be higher. The mixed domains emerges more consistently with values of internal heat of 2×10^{-11} W kg^{-1} (Fig. 12D). This agrees with the work of Lenardic (2006) and Lenardic et al. (2005, 2003) and Capitanio et al. (2019a), where two domains emerge within the same lithosphere: a domain of thick, poorly mobile lid with low-heat flux, and a domain of thinner lid where heat flux and, consequently, mobility are higher. This spatial and temporal evolution mitigates the constraints imposed by Korenaga's model, which may otherwise result in a complete shutdown of surface motions.

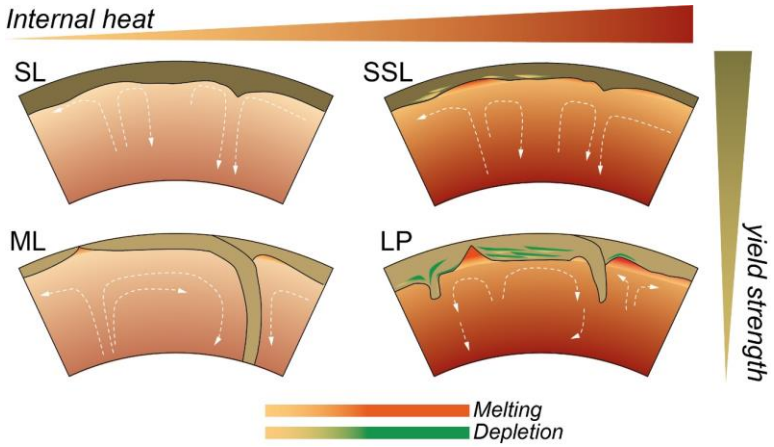

Figure 10. Sketch of the regimes in the models. For lower values of internal heat, the models develop a sluggish lid (SL) and a mobile lid (ML) regimes, for high and low yield strength, respectively. Melting and depletion is negligible in these models. As internal heat increases, the average mantle temperature increase, and so does melting and depletion degree (red- and green-to- yellow colour bars). For high strength, favourable to the SL regime, the thermal lid is thinner, yet small volumes of depleted mantle stabilise the lid, which evolves from a sluggish to stagnant lid (SSL regime). Lower lithospheric strength reproduces condition of ML, with higher mobility, large volumes of depleted lithosphere and high depletion degree. However, this latter eventually stabilised the lid. This regime is called lid-and-plate (LP).

Our modelling reproduces these thermal evolution trends and shows contrasting regimes for Phanerozoic low and Precambrian high internal heat production, respectively, controlled by: a thermal boundary layer, which buoyancy and viscosity are temperature-dependent, and a thermochemical boundary layer, where buoyancy and viscosity are depletion-dependent instead (Fig. 10). Models with low internal heat production tend to follow a "classical" scaling law, where the lithosphere is the thermal boundary, reproducing Proterozoic-Phanerozoic cooling rates of –50 to –100 ˚C/Gyr constrained by non-arc basalt melting (Herzberg et al., 2010). Instead, for large internal heat, the lithosphere differentiates in a thicker and more rigid thermochemical boundary, reproducing a strong increase in mantle temperature > 100 ˚C/Gyr in agreement with those inferred for the Archean.

It is important to note that the transition between the two stable branches with $\beta < 0$ and $\beta > 0$ may not occur as shown in figure 9. This transition, also known as Tectono-Convective

Transition Window, depends on the rate at which the convection readjusts to decreasing internal heat rate (Korenaga, 2017; Lenardic and Crowley, 2012; Moore and Lenardic, 2015; Weller and Lenardic, 2012), which is not addressed here. Our transition models show features of both the end members, shown in Fig. 12D.

4.2. Constraints on the tectonics of the early Earth

Reconstructing the tectonic regimes of the early Earth mostly relies on geochemical and petrological constraints on mantle temperatures and melt degrees. These are recovered using remnant basalts, picrites and komatiites in cratons, and complementary lithospheric mantle peridotites, found in xenoliths (Griffin et al., 2003; Griffin et al., 1999; Herzberg et al., 2007; Lee et al., 2011; Pearson, 1999; Pearson and Wittig, 2008). The melting temperature of basalts is reflective of the mantle potential temperature, where initial melt is generated, albeit it does not reflect average values. Inferred Archean temperatures are between 1470 and 1640 ˚C, and steadily increase throughout the eon (Herzberg et al., 2010) (Fig 11). Largest temperatures are constrained by komatiitic melts, in excess of 1700 ˚C (Fig 11, dashed box), although these are likely indicative of different tectonic settings. Variable depletion degrees are constrained from the rock record, reaching maximum values of 0.3 to 0.45 (Lee et al., 2011). The temperature trend reverts after the Archean onwards, with potential temperatures steadily decreasing by secular cooling rate bracketed between 50 and 100 ˚C Gyr^{-1} (Jaupart et al., 2015). Mantle potential temperatures range between 1600 and ~1450 ˚C by the end of Proterozoic, and reach present-day mantle potential temperatures of 1350 ± 50 ˚C (Fig. 11, brown and blue boxes), while maximum depletion degrees decrease to < ~0.3 and to present-day values of ~0.08.

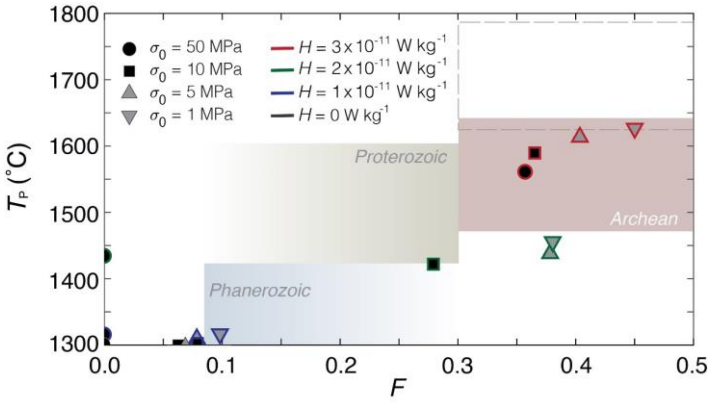

Figure 11. Maximum potential temperature vs largest depletion degree *F*, for the models and from cratons observations for Archean (pink box), Proterozoic (green box) and Phanerozoic (blue box). Dashed line for the values inferred from komatiites (see text).

Albeit simplified, our models' potential temperatures and melt degrees match the inferred conditions of the Earth for yield strength comparable to present-day's. Models with $H \geq 2 \times 10^{-11}$ W kg^{-1} reproduce conditions of the Precambrian. The models with largest internal heat tested, $H = 3 \times 10^{-11}$ W kg^{-1}, reach temperatures between 1560 and 1620 ˚C, which fall in the range of the Archean (Fig. 11, red rim symbols). The maximum depletion degrees in these models also agree with the observations, ranging between 0.36 and ~045, increasing for decreasing yield strength of the lithosphere, from 50 MPa to 1 MPa, respectively. Models with moderate internal heat, $H = 2 \times 10^{-11}$ W kg^{-1}, show temperatures tightly around ~1450 ˚C (Fig. 11, green rim symbols), in agreement with those inferred for the end of the Proterozoic, although the temperatures in these models might be too dependent on the initial conditions chosen. However, the depletion degree in these models varies largely, from 0.38 to 0, for decreasing lithospheric strength. Models with $H \leq 1 \times 10^{-11}$ W kg^{-1} all reproduce temperatures and depletion degrees in agreement with the Phanerozoic values (Fig. 11, blue and black rims), for $\sigma_0 > 20$ MPa. While this emphasises the controls of lithospheric thinning, favoured by decreased lithospheric strength, it suggests that only for values of $\sigma_0 \leq 10$ MPa the depletion degrees in the Precambrian can be matched.

Additionally, models with lithospheric strength comparable to today's best match the scarce geological record of the Archean. Beside large melting volumes and depleted lithosphere, plate margins features, akin to convergent and divergent boundaries, are commonly documented in cratons (Griffin et al., 2003; Griffin et al., 1999; Simon et al., 2007; van Hunen and Moyen, 2012; Van Kranendonk et al., 2007). Melting beneath very thin lithosphere is recorded in the Kaapvaal craton (Simon et al., 2007), with large volumes of depleted continental lithospheric mantle, ~3.5 – 3.2 Ga. Subsequently, short-lived subduction-like environments, ~2.9 Ga, are recorded. In the Pilbara craton (Van Kranendonk et al., 2007), a similar formation of mantle melting and depletion is recorded for the period 3.8 – 3.2 Ga, with arc-like magmatism, in episodes of 20 to 50 Myr, interpreted to reflect short-lived subduction and episodic rifting, with voluminous TTG-like crustal melting. Similar evolution is proposed for the Inukjuak domain, Québec (Caro et al., 2017), were evidence of Hadean recycling and stabilisation of the

803 Eoarchean lid, point towards an initial mobility later stabilised into a sluggish lid. Zircon
804 analyses support the idea that crustal reworking was ongoing since the Hadean (Harrison, 2009;
805 Kemp et al., 2010; Turner et al., 2014). Similarly, crustal records suggest complete recycling of
806 the Hadean crust, followed by subdued recycling of the Archean crust before 3 Ga (Dhuime et
807 al., 2015). The spatial distribution of this evidence, although poorly constrained, illustrates
808 domains with clustered plate tectonics-like features (Van Kranendonk, 2010).

809 Similar features are reproduced by our models in the lid-and-plate regime, with areas of
810 stable lid and others with larger mobility, in a regime allowing for episodic, yet localised
811 mobility. In the model's regime, large recycling and mantle depletion degrees and volumes occur
812 early in the cratons' evolution. The negative feedback between dehydration stiffening and
813 lithospheric yielding accounts for short-lived lithospheric convergent and divergent zones, with
814 large melting and large crustal mobility. In the subsequent stabilisation stage, further recycling,
815 although minor, and reworking are allowed, while plate margins-like features remain embedded
816 within the lid, preserving them. The occurrence of these plate-margin features within the lid,
817 however, promotes stiffening and their preservation through geologic time, preventing
818 continuous destructive plate margin processes to operate, as is the case today.

819 Additional support comes from theoretical and modelling arguments. The lid-and-plate
820 regime presents a stage with mobility and could have been viable on the early Earth (Höink et
821 al., 2013; Jellinek and Jackson, 2015). Subduction-like processes could have been viable since
822 the Hadean (Foley et al., 2014), although episodic (O'Neill et al., 2007; van Hunen and Moyen,
823 2012), while localised rifting can also emerge as a stable feature (Rozel et al., 2015).
824 Additionally, the remnants of Archean cratons rule out episodic complete overturns of the lid
825 (O'Neill et al., 2007), which would have obliterated any record, instead. The conditions
826 favourable to mobile lid regime in the early Earth, as those for the LP regime, are necessary
827 conditions for planetary evolution to plate tectonics (Lenardic and Crowley, 2012; Weller and
828 Lenardic, 2012).

829 Melt extraction and advection through the lithosphere may have critically mitigated the
830 excess heat of the mantle (Moore and Webb, 2013) and facilitate the formation of plate margins
831 (Jain et al., 2019; Lourenço et al., 2018; Rozel et al., 2017). This can be compared to the early
832 stage of large heat release in the models presented here indicated by evolution in the melt, and
833 therefore melt depletion. Heat transfer and plutonism might also play a role in mobilising the lid,

sustaining short lived plate margins with convergence and overturn (Lourenço et al., 2018). Although we do not model plutonic emplacement and heat advection, our models are complementary to the squishy lid and plutonic-squishy lid regimes (Lourenço et al., 2018; Rozel et al., 2017): while these earlier works focused on the role of the extracted melt, we focus here on the role of the residue left by melt extraction.

Finally, although the LP regime ends with a rather stagnant lid-type environment, it differ substantially from the thermal boundary layer's stagnant lid (e.g., Moresi and Solomatov, 1998), as the LP emerges at low strength, favourable to a mobile lid regime, instead. The episodic mobility, evolution, thickness, heat flow and melt depletion volumes and degrees of the thermochemical lithosphere are different from that predicted by the thermal boundary layer's stagnant lid. While this regime might occur on other rocky planets (e.g., Moresi and Solomatov, 1998; Stern et al., 2018), the geological and geodynamic evidence suggest that the tectonic regime of the early Earth was never uniformly nor constantly stagnant.

4.3.Speculations of the tectonics transitions on Earth

The models presented provide insights into the tectonics of the Earth under conditions inferred for the Precambrian, supporting some speculation on the tectonics transition. This section addresses the question on how this might have happened, rather than when.

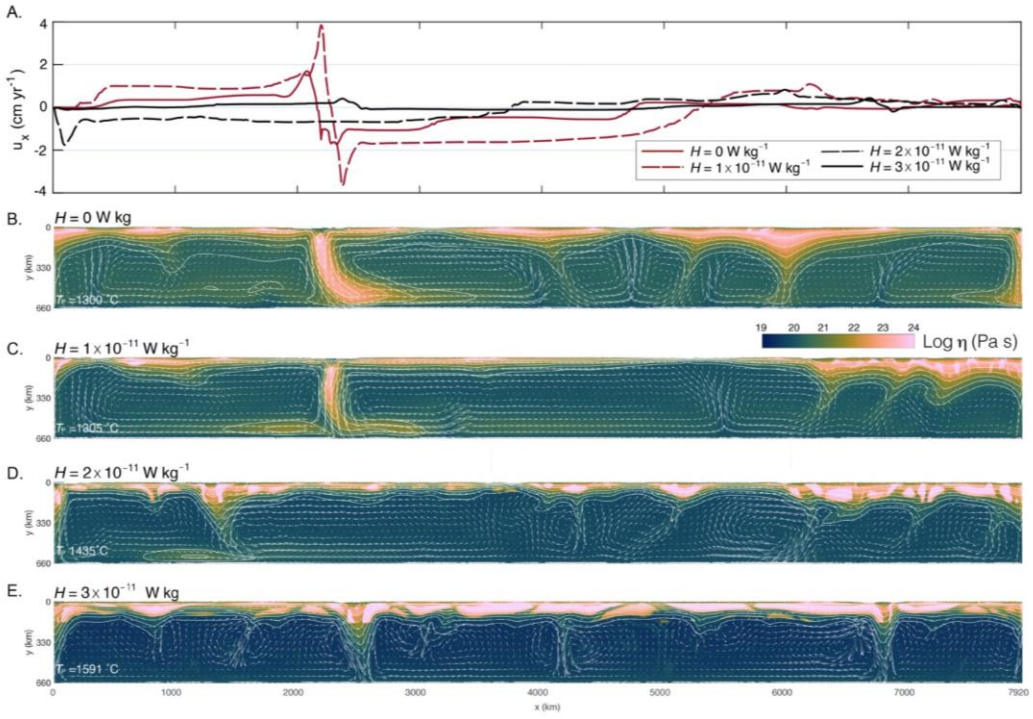

Figure 12. Ideal evolution of the tectonics on Earth illustrated by models with the same yield strength (σ_0 = 10 MPa) and decreasing values of internal heat generation H. (A) surface velocity of the models shows similar features with convergence and divergence, although for values ≥ 2 × 10^{-11} W kg^{-1} surface motions are < 1 cm yr^{-1}, reaching velocity in the order of few cm yr^{-1} for lower internal heat. (B and C) similar features develop for $H \leq 1 \times 10^{-11}$ W kg^{-1}, with convergent margins and subduction, with the lithosphere thickening for decreasing largest mantle potential temperature (T_P). For higher internal heat $H \geq 2 \times 10^{-11}$ W kg^{-1}, the trend inverts and the lithosphere thickens for increasing mantle temperature, with larger volumes of depleted mantle embedded in the lithosphere.

The models with Phanerozoic internal heat values, and yield strength of 10 MPa (Fig. 12A-C), reproduce the mobile lid regime, with features akin to modern plate tectonics, with melting, mantle temperatures, larger surface velocity, divergence and convergence, where ridges and subduction zones form, respectively. These lithospheric yield strength values are compatible with laboratory-constrained values of cohesion and lower values used in numerical modelling (see Gerya, 2009). Then, increasing the internal heat to Precambrian values, with yield strength being the same (Fig. 12D, E), that is ML regime conditions, the models develop higher mantle temperatures and depletion degrees to stabilise the lid and suppresses mobility and plate tectonics-like features. Surface motions are rather small, <1 cm yr^{-1}, and show features of small rigid proto-plates, divergent/convergent zones, rather uniform lid thickness and heat flow. Although the yield strength is low enough to allow the fragmentation of the lid, the negative feedback between yielding and melt depletion-stiffening allows only episodic, short-lived subduction and ridges (Fig. 12A, black lines). In this sense the transition of the tectonics between a rigid lid and a mobile, fragmented lithosphere occur under the same lithospheric strength, yet the thermochemical differentiation leads to a different regime.

These results agree with a range of published modelling efforts (Stein et al., 2004; Tackley, 2000) and emphasise the control of thermomechanical differentiation on the tectonics' transition. In previous works, the tectonics transition from a stagnant lid to a mobile lid regime implies changed conditions, that is lithospheric strength or viscosity decreasing in time. However, the thermal boundary layer approach does not explain such a transition, instead it leads to the opposite conclusion: the Earth should have transitioned from plate tectonics to a present-

884 day stagnant lid (Sleep, 2000). Here, we have shown that the conditions determining the regime
885 did not change on Earth, that is the yield strength was unlikely higher in the early Earth, then the
886 tectonics' transition is due to the disappearance of the thermochemical lithosphere, with the
887 waning of large depletion, following radioactive heat decay, allowing plate margins to form and
888 modern plate tectonics to start. In this frame, the ideal evolution of Earth's tectonics is not that of
889 a transition among different regimes, but rather that of an evolution from a thermochemical
890 boundary layer, which buoyancy and viscosity are depletion-dependent, to a thermal boundary
891 layer, which buoyancy and viscosity are temperature-dependent. The switch from the early Earth
892 thermochemical to present-day thermal lithosphere, implies an inversion of the stiffness
893 dependence on temperature (Fig. 12). The evolution proposed here has elements in common with
894 Sleep (2000), where the mobility of an early Earth is reduced by the formation of depleted, stiffer
895 mantle beneath plate margins, the "trench lock", favouring the increase of internal temperatures
896 and, eventually, a stagnant-lid. Then, conditions for kick starting of plate tectonics is the
897 vanishing of melt-depletion. Additionally, Korenaga, 2006, introduces the dehydration stiffening
898 hypothesis suggesting a "sluggish plate tectonics" active in the Archean. This regime requires
899 subdued, yet continuously operating plate tectonics, throughout Earth's history. Here, using an
900 implementation based on Korenaga, 2006, we found that the thermochemical differentiation
901 leads to a spatially localised and time-dependent evolution, best in agreement with the geological
902 record. In this sense, the lid-and-plate regime reconciles with the conditions favourable to plate
903 tectonics suggested by Sleep, 2000, and Korenaga, 2006, however, for decreasing values of
904 internal heat, yet $\geq 2 \times 10^{-11}$ W kg^{-1} (Fig. 12D, E) the distribution of depleted lithospheric
905 mantle decreases, and a mixed mode with different domains of thin and thick lid emerge, in
906 agreement with the "sluggish lid" regime proposed by Lenardic. This regime might have been
907 viable during the transition, although thermochemical differentiation must be invoked to explain
908 the formation of cratons (Capitanio et al., 2020).

909 Heterogeneities formed during lithosphere differentiation may additionally help the
910 tectonics transition. The impingement of plumes onto the rigid lid may have triggered
911 lithospheric foundering (Davaille et al., 2017; Gerya et al., 2014), while in the Hadean Earth
912 fragmentation of the lid could have followed very large bolide impacts (>~700 km, O'Neill et al.,
913 2017). While these may have provided excess forcing, the heterogeneities shown here, as well as
914 similar inherited damage zones (Foley, 2018), may have focused stress, facilitating yielding

along lithospheric discontinuities (e.g., Bercovici and Ricard, 2014; Rey et al., 2014), reactivating these "paleo-suture" zones into plate boundaries, kickstarting modern plate tectonics. Then the conditions for high mobility allowed the persistence of stable plate margins.

Conclusions

Modelling mantle convection under present-day and early Earth internal heat conditions provides viable proxies for the tectonic regimes that may have operated through Earth's evolution. Under Phanerozoic or present-day conditions, melting, melt extraction and stiffening of the residual mantle have a negligible impact on the convection regime. Then, the Earth's regime and the viability of plate tectonics depends on the ability of the thermal boundary layer to yield, forming plate margins, such as subduction zones and ridges. However, when internal heat production is comparable to that in the early Earth, melting degrees increase, leaving large volumes of depleted, therefore stiffer residue at shallow depth. The lithosphere's thermochemical differentiation has a relevant impact on the evolution of Archean regimes, which substantially differ from that of the Phanerozoic. The initial mobility of the lid is progressively confined by the growing thickness of depleted, stiffer lithospheric mantle, until it fully stabilises, preserving volumes of high-degree melting residue and fossil tectonic features from further recycling. All models with present-day lithospheric strength or lower, follow the two-steps evolution from an initially mobile lithosphere to a later stabilisation, into a poorly mobile, thick lid, in a regime called *lid-and-plate*. The geological record of large melting and depletion, reworking and in parts recycling, episodic subduction and rifting, provides support to the viability of a regime dominated by the negative feedback between low strength, favouring mobility and large melting, and progressive stiffening, suppressing mobility and preserving the lithosphere into cratons. The models suggest a thermal budget in the Precambrian dominated by depletion of a thermochemical boundary layer, which breaks the dependence of the conductive layer thickness on the mantle temperatures, in agreement with inferred thermal evolution. We show that lithosphere thermochemical differentiation is a process of mantle convection that cannot be neglected when addressing the regime of the early Earth. We speculate that the yield strength conditions favourable to a mobile lid regime never changed, yet the thermochemical differentiation stabilised the lithosphere, suppressing plate margin formation, until lower values

of internal heat were reached and depletion vansished, when plate margins could evolve into stable features of modern plate tectonics.

Data availability

All data are generated using underworldcode/underworld2: v2.8.1b (Version v2.8.1b). Zenodo. http://doi.org/10.5281/zenodo.3384283.

Acknowledgment

We acknowledge support from *Australian Research Council* grants FT170100254 (to Capitanio) and FL160100168 (to Cawood). We acknowledge the provision of resources and services from the *National Computational Infra-structure* (NCI), which is supported by the Australian Government.

References

Arndt, N.T., Lewin, E., Albarède, F., 2002. Strange partners: formation and survival of continental crust and lithospheric mantle in: Fowler, C.M.R., Ebinger, C.J., Hawkesworth, C.J. (Eds.), The Early Earth: Physical, Chemical and Biological Development. Geol. Soc. Spec. Publ., London, pp. 91-103.

Bédard, J.H., Harris, L.B., 2014. Neoarchean disaggregation and reassembly of the Superior craton. Geology 42, 951–954.

Bercovici, D., Ricard, Y., 2014. Plate tectonics, damage and inheritance. Nature 508, 513.

Bickle, M.J., 1986. Implications of melting for stabilisation of the lithosphere and heat loss in the Archaean. Earth and Plan. Lett. 80, 314-324.

Buffett, B.A., Rowley, D.B., 2006. Plate bending at subduction zones: Consequences for the direction of plate motions. Earth Plan. Sci. Let. 245, 359-364.

Capitanio, F.A., Morra, G., 2012. The bending mechanics in a dynamic subduction system: constraints from numerical modeling and global compilation analysis. Tectonophysics 522-523, 224-234.

Capitanio, F.A., Morra, G., Goes, S., 2009. Dynamics of plate bending at the trench and slab-plate coupling. Geochem. Geophys. Geosyst. 10, doi:10.1029/2008GC002348.

976 Capitanio, F.A., Nebel, O., Cawood, P.A., 2020. Thermochemical lithosphere differentiation and
977 the origin of cratonic mantle. Nature Accepted.
978 Capitanio, F.A., Nebel, O., Cawood, P.A., Weinberg, R.F., Chowdhury, P., 2019a. Reconciling
979 thermal regimes and tectonics of the early Earth. Geology 47,
980 https://doi.org/10.1130/G46239.46231.
981 Capitanio, F.A., Nebel, O., Cawood, P.A., Weinberg, R.F., Clos, F., 2019b. Lithosphere
982 differentiation in the early Earth controls Archean tectonics. Earth Plan. Sci. Lett. 525,
983 https://doi.org/10.1016/j.epsl.2019.115755.
984 Caro, G., Morino, P., Mojzsis, S.J., Cates, N.L., Bleeker, W., 2017. Sluggish Hadean
985 geodynamics: Evidence from coupled 146,147Sm–142,143Nd systematics in Eoarchean
986 supracrustal rocks of the Inukjuak domain (Québec). Earth Plan. Sci. Lett. 457, 23-37.
987 Cawood, P.A., Hawkesworth, C.J., Pisarevsky, S., Dhuime, B., Capitanio, F.A., Nebel, O., 2018.
988 Geological archive of the onset of plate tectonics. Phil. Trans. R. Soc. A 376.
989 Cawood, P.A., Kröner, A., Collins, W.J., Kusky, T.J., Mooney, W.D., Windley, B.F., 2009.
990 Accretionary orogens through Earth history, in: Cawood, P.A., Kröner, A. (Eds.), Earth
991 Accretionary Systems in Space and Time. The Geol. Soc., London, pp. 1-36.
992 Chowdhury, P., Gerya, T.V., Chakraborty, S., 2017. Emergence of silicic continents as the lower
993 crust peels o on a hot plate-tectonic Earth. Nat. Geoscience 10, 698-703.
994 Christensen, U.R., 1985. Thermal Evolution Models for the Earth. J. Geophys. Res. 90, 2995-
995 3007.
996 Conrad, C.P., Hager, B.H., 1999. The thermal evolution of an earth with strong subduction
997 zones. Geophys. Res. Lett. 26, 3041-3044.
998 Crameri, F., 2018. Scientific colour maps. Zenodo, http://doi.org/10.5281/zenodo.1243862.
999 Davaille, A., Jaupart, C., 1993. Transient high-Rayleigh-number thermal convection with large
1000 viscosity variations. J. Fluid Mech. 253, 141–166.
1001 Davaille, A., Smrekar, S.E., Tomlinson, S., 2017. Experimental and observational evidence for
1002 plume-induced subduction on Venus. Nat. Geoscience 10, 349-355.
1003 Davies, G.F., 1980. Thermal Histories of Convective Earth Models and Constraints on
1004 RadiogenicHeat Productionin the Earth. J. Geophys. Res. 85, 2517-2530.
1005 Davies, G.F., 2009. Effect of plate bending on the Urey ratio and the thermal evolution of the
1006 mantle. Earth Plan. Sci. Let. 287, 513-518.

1007 de Wit, M., Furnes, H., MacLennan, S., Doucouré, M., Schoene, B., Weckmann, U., Martinez,
1008 U., Bowring, S., 2018. Paleoarchean bedrock lithologies across the Makhonjwa Mountains of
1009 South Africa and Swaziland linked to geochemical, magnetic and tectonic data reveal early plate
1010 tectonic genes flanking subduction margins. Geoscience Frontiers 9, 603-665.
1011 Dhuime, B., Wuestefeld, A., Hawkesworth, C.J., 2015. Emergence of modern continental crust
1012 about 3 billion years ago. Nat. Geoscience 8, doi: 10.1038/NGEO2466.
1013 Dunnberg, J., Heister, T., 2016. Compressible magma/mantle dynamics: 3-D, adaptive
1014 simulations in ASPECT. Geophys. J. Int. 207, 1343-1366.
1015 Fischer, R., Gerya, T.V., 2016. Early Earth plume-lid tectonics: A high-resolution 3D numerical
1016 modelling approach. J. Geodyn. 100, 198-214.
1017 Foley, B.J., 2018. The dependence of planetary tectonics on mantle thermal state: applications to
1018 early Earth evolution. Phil. Trans. R. Soc. A 376, http://dx.doi.org/10.1098/rsta.2017.0409.
1019 Foley, B.J., Bercovici, D., 2014. Scaling laws for convection with temperature-dependent
1020 viscosity and grain-damage. Geophys. J. Int. 199, 580-603.
1021 Foley, B.J., Bercovici, D., Elkins-Tanton, L.T., 2014. Initiation of plate tectonics from post-
1022 magma ocean thermochemical convection. J. Geophys. Res. 119, 8538–8561.
1023 Gardiner, N.J., Kirkland, C.L., Hollis, J.A., Cawood, P.A., Nebel, O., Szilas, K., Yakymchuk, C.,
1024 2020. North Atlantic Craton architecture revealed by kimberlite-hosted crustal zircons. Earth and
1025 Plan. Lett. 534, https://doi.org/10.1016/j.epsl.2020.116091.
1026 Gerardi, G., Ribe, N.M., Tackley, P.J., 2019. Plate bending, energetics of subduction and
1027 modeling of mantle convection: A boundary element approach. Earth Plan. Sci. Lett. 515, 47-57.
1028 Gerya, T.V., 2009. Introduction to numerical geodynamical modelling. Cambridge University
1029 Press.
1030 Gerya, T.V., 2014. Precambrian geodynamics: Concepts and models. Gond. Res. 25, 442-463.
1031 Gerya, T.V., Stern, R.J., Baes, M., Sobolev, S.V., Whattam, S.A., 2014. Plate tectonics on the
1032 Earth triggered by plume-induced subduction initiation. Nature 527, 221-225.
1033 Griffin, W.L., O'Reilly, S.Y., Abe, N., Aulbach, S., Davies, R.M., Pearson, N.J., Doyle, B.J.,
1034 Kivi, K., 2003. The origin and evolution of Archean lithospheric mantle. Precambrian Res. 127,
1035 19-41.
1036 Griffin, W.L., O'Reilly, S.Y., Ryan, C.G., 1999. The composition and origin of subcontinental
1037 lithospheric mantle, in: Fei, Y., Bertka, C.M., Mysen, B.O. (Eds.), Mantle petrology: Field

observations and high-pressure experimentation: A tribute to Francis R. (Joe) Boyd. The Geochemical Society, Houston, Texas, pp. 13–43.

Harrison, T.M., 2009. The Hadean Crust: Evidence from >4 Ga Zircons. Annu. Rev. Earth Planet. Sci. 37, 479–505.

Herzberg, C., Asimow, P.D., Arndt, N., Niu, Y., Lesher, C.M., Fitton, J.G., Cheadle, M.J., Saunders, A.D., 2007. Temperatures in ambient mantle and plumes: constraints from basalts, picrites, and komatiites. Geochem. Geophys. Geosys. 8.

Herzberg, C., Condie, K., Korenaga, J., 2010. Thermal history of the Earth and its petrological expression. Earth Plan. Sci. Lett. 292, 79–88.

Hirth, G., Kohlstedt, D.L., 1996. Water in the oceanic upper mantle: implications for rheology, melt extraction and the evolution of the lithosphere Earth Plan. Sci. Lett. 144, 93-108.

Höink, T., Lenardic, A., Jellinek, A.M., 2013. Earth's thermal evolution with multiple convection modes: A Monte-Carlo approach. Phys. Earth Planet. Int. 221, 22-26.

Ito, G., Shen, Y., Hirth, G., Wolfe, C.J., 1999. Mantle flow, melting, and dehydration of the Iceland mantle plume. Earth Plan. Sci. Lett. 165, 81-96.

Jain, C., Rozel, A.B., Tackley, P.J., Sanan, P., Gerya, T.V., 2019. Growing primordial continental crust self-consistently in global mantle convection models. Gond. Res. 73, 96-12.

Jaupart, C., Labrosse, S., Lucazeau, F., Mareschal, J.C., 2015. Temperatures, Heat, and Energy in the Mantle of the Earth, in: Schubert, G. (Ed.), Treatise on Geophysics. Elsevier, Amsterdam, pp. 223-270.

Jellinek, A.M., Jackson, M.G., 2015. Connections between the bulk composition, geodynamics and habitability of Earth. Nat. Geoscience 8, 587-593.

Johnson, T.E., Brown, M., Kaus, B.J.P., VanTongeren, J.A., 2014. Delamination and recycling of Archaean crust caused by gravitational instabilities. Nat. Geoscience 7, 47-52.

Jordan, T.H., 1988. Structure and Formation of the Continental Tectosphere. J. of Petr., 11-37.

Katz, R.F., Spiegelman, M., Langmui, C.H., 2003. A new parameterization of hydrous mantle melting. Geochem. Geophys. Geosys. 4, doi:10.1029/2002GC000433.

Kemp, A.I.S., Wilde, S.A., Hawkesworth, C.J., Coath, C.D., Nemchin, A., Pidgeon, R.T., Vervoort, J.D., DuFrane, S.A., 2010. Hadean crustal evolution revisited: New constraints from Pb–Hf isotope systematics of the Jack Hills zircons. Earth Plan. Sci. Lett. 296, 45-56.

1068 Kohlstedt, D.L., Hansen, L.N., 2015. Constitutive Equations, Rheological Behavior, and
1069 Viscosity of Rocks, in: Schubert, G. (Ed.), Treatise on Geophysics, pp. 441-472.
1070 Korenaga, J., 2003. Energetics of mantle convection and the fate of fossil heat. Geophys. Res.
1071 Lett. 30, 1437-1440.
1072 Korenaga, J., 2006. Archean Geodynamics and the Thermal Evolution of Earth, in: Benn, K.,
1073 Mareschal, J.C., Condie, K. (Eds.), Archean Geodynamics and Environments. American
1074 Geophysical Union, p. 10.1029/GM1164.
1075 Korenaga, J., 2013. Initiation and Evolution of Plate Tectonics on Earth: Theories and
1076 Observations. Annu. Rev. Earth Planet. Sci. 41, 117-151.
1077 Korenaga, J., 2017. Pitfalls in modeling mantle convection with internal heat production. J.
1078 Geophys. Res. 122, 4064–4085.
1079 Lamb, S.H., 1984. Geology of part of the Archaean Barberton Greenstone Belt. Cambridge
1080 Press.
1081 Lee, C.-T.A., Luffi, P., Chin, E.J., 2011. Building and Destroying Continental Mantle. Annu.
1082 Rev. Earth Planet. Sci. 39, 59-90.
1083 Lenardic, A., 2006. Continental Growth and the Archean Paradox, in: Benn, K., Mareschal, J.C.,
1084 Condie, K. (Eds.), Archean Geodynamics and Environments. American Geophysical Union, p.
1085 10.1029/1164GM1004.
1086 Lenardic, A., 2018. The diversity of tectonic modes and thoughts about transitions between
1087 them. Phil. Trans. R. Soc. A 376, 20170416.
1088 Lenardic, A., Crowley, J.W., 2012. On the notion of well-defined tectonic regimes for terrestrial
1089 planets in this solar system and others. Astrophys. J. 755, doi:10.1088/0004-
1090 1637X/1755/1082/1132.
1091 Lenardic, A., Moresi, L.N., Jellinek, A.M., Manga, M., 2005. Continental insulation, mantle
1092 cooling, and the surface area of oceans and continents. Earth Plan. Sci. Let. 234, 317-333.
1093 Lenardic, A., Moresi, L.N., Mülhaus, H., 2003. Longevity and stability of cratonic lithosphere:
1094 Insights from numerical simulations of coupled mantle convection and continental tectonics. J.
1095 Geophys. Res. 108, doi:10.1029/2002JB001859.
1096 Leng, W., Zhong, S., 2010. Constraints on viscous dissipation of plate bending from
1097 compressible mantle convection. Earth Plan. Sci. Let. 297, 154-164.

1098 Lourenço, D.L., Rozel, A.B., Gerya, T.V., Tackley, P.J., 2018. Efficient cooling of rocky planets
1099 by intrusive magmatism. Nat. Geoscience 11, 322-327.
1100 McKenzie, D., Bickle, M.J., 1988. The Volume and Composition of Melt Generated by
1101 Extension of the Lithosphere. J. of Petrology 29, 625-679.
1102 Mei, S., Kohlstedt, D.L., 2000. Influence of water on plastic deformation of olivine aggregates. J.
1103 Geophys. Res 105, 21457-21469.
1104 Moore, W.B., Lenardic, A., 2015. The efficiency of plate tectonics and nonequilibrium
1105 dynamical evolution of planetary mantles. Geophys. res. Lett. 42, 9255–9260.
1106 Moore, W.B., Webb, A.G., 2013. Heat-pipe Earth. Nature 501, 501–505.
1107 Moresi, L., Quenette, S., Lemiale, V., C., M., Appelbe, B., Mülhaus, H.B., 2007. Computational
1108 approaches to studying non-linear dynamics of the crust and mantle. Phys. Earth Plan. Int. 163,
1109 69-82.
1110 Moresi, L., Solomatov, V.S., 1998. Mantle convection with a brittle lithosphere: thoughts on the
1111 global tectonic styles of the Earth and Venus. Geophy. J. Int. 133, 669-682.
1112 Moresi, L.N., Solomatov, V.S., 1995. Numerical investigation of 2D convection with extremely
1113 large viscosity variations. Phys. of Fluids 7, 2154-2162.
1114 Nebel, O., Capitanio, F.A., Moyen, J.-F., Weinberg, R.F., Clos, F., Nebel-Jacobsen, Y.J.,
1115 Cawood, P.A., 2018. 2018 When crust comes of age: on the chemical evolution of Archaean,
1116 felsic continental crust by crustal drip tectonics. Phil. Trans. R. Soc. A 376, 20180103.
1117 O'Neill, C., Lenardic, A., Moresi, L.N., Torsvik, T.H., Lee, C.-T.A., 2007. Episodic Precambrian
1118 subduction. Earth Plan. Sci. Lett. 262, 552-562.
1119 O'Neill, C., Marchi, S., Zhang, S., Bottke, W., 2017. Impact-driven subduction on the Hadean
1120 Earth. Nat. Geoscience 10, 793-797.
1121 Pearson, D.G., 1999. The age of continental roots. Lithos 48, 171-194.
1122 Pearson, D.G., Wittig, N., 2008. Formation of Archaean continental lithosphere and its
1123 diamonds: the root of the problem. J. Geol. Soc. London 165, 895-914.
1124 Phipps-Morgan, J., 1997. The generation of a compositional lithosphere by mid-ocean ridge
1125 melting and its effect on subsequent off-axis hotspot upwelling and melting. Earth Plan. Sci.
1126 Lett. 146, 213-232.
1127 Piccolo, A., Palin, R.M., Kaus, B.J.P., White, R.W., 2019. Generation of Earth's early continents
1128 from a relatively cool Archean mantle. Geochem. Geophys. Geosys. 20, 1679-1697.

1129 Pinkerton, H., Stevenson, R.J., 1992. Methods of determining the rheological properties of
1130 magmas at subliquidus temperatures. J. Volc. Geother. Res. 53, 47-66.
1131 Rey, P.F., Coltice, N., Flament, N., 2014. Spreading continents kick-started plate tectonics.
1132 Nature 513, 405-408.
1133 Rolf, T., Capitanio, F.A., Tackley, P.J., 2018. Constraints on mantle viscosity structure from
1134 continental drift histories in spherical mantle convection models. Tectonophy. 746, 339-351.
1135 Rozel, A., Golabek, G.J., Näf, R., Tackley, P.J., 2015. Formation of ridges in a stable lithosphere
1136 in mantle convection models with a viscoplastic rheology. Geophys. Res. Lett. 42, 4770-4777.
1137 Rozel, A.B., Golabek, G.J., Jain, C., Tackley, P.J., Gerya, T.V., 2017. Continental crust
1138 formation on early Earth controlled by intrusive magmatism. 545, 332 - 335.
1139 Schutt, D.L., Lesher, C.E., 2006. Effects of melt depletion on the density and seismic velocity of
1140 garnet and spinel lherzolite. J. Geophys. Res. 111, B05401.
1141 Simon, N.S.C., Carlson, R.W., Pearson, D.G., Davis, G.R., 2007. The Origin and Evolution of
1142 the Kaapvaal Cratonic Lithospheric Mantle. J. Petrol. 48, 589-625.
1143 Sizova, E., Gerya, T.V., Stüwe, K., Brown, M., 2015. Generation of felsic crust in the Archean:
1144 A geodynamic modeling perspective. Precambrian Res. 2771, 198-224.
1145 Sleep, N.H., 2000. Evolution of the mode of convection within terrestrial planets. J. Geophys.
1146 Res. 105, 17,563-517,578.
1147 Solomatov, S., 1995. Scaling of temperature- and stress- dependent viscosity convection. Physics
1148 of Fluids 7, https://doi.org/10.1063/1061.868624.
1149 Stein, C., Schmalzl, J., Hansen, U., 2004. The effect of rheological parameters on plate
1150 behaviour in a self-consistent model of mantle convection. Phys. Earth Planet. Int. 142, 225-255.
1151 Stern, R.J., 2018. The evolution of plate tectonics. Phil. Trans. R. Soc. A 376, doi:
1152 10.1098/rsta.2017.0406.
1153 Stern, R.J., Gerya, T., Tackley, P.J., 2018. Stagnant lid tectonics: Perspective from silicate
1154 planets, dwarf planets, large moons, and large asteroids. Geosci. Frontiers 9, 103-119.
1155 Tackley, P.J., 1998. Self-consistent generation of tectonic plates in three-dimensional mantle
1156 convection. Earth Plan. Sci. Let. 157, 9-22.
1157 Tackley, P.J., 2000. Self-consistent generation of tectonic plates in time-dependent. three-
1158 dimensional mantle convection simulation 2. Strain weakening and asthenosphere. Geoc.
1159 Geophy. Geosys. 1, 2000GC000036.

Turcotte, D.L., Oxburgh, E.R., 1967. Finite amplitude convection cells and continental drift. J. Fluid Mech. 28, 29-42.

Turcotte, D.L., Schubert, G., 1982. Geodynamics, application of continuum mechanics to geological problems. John Wiley & Sons, New York.

Turner, S., Rushmer, T., Reagan, M., Moyen, J.F., 2014. Heading down early on? Start of subduction on Earth. Geology 42, 139-142.

van Heck, H.J., Tackley, P.J., 2008. Planforms of self-consistently generated plates in 3D spherical geometry. Geophys. Res. Let. 35, L19312.

van Hunen, J., Moyen, J.F., 2012. Archean Subduction: Fact or Fiction? Annu. Rev. Earth Planet. Sci. 40, 195–219.

Van Kranendonk, M.J., 2010. Two types of Archean continental crust: Plume and Plate Tectonics on early Earth. Am. J. of Sci. 310, 1187-1209.

Van Kranendonk, M.J., Smithies, R.H., Hickman, A.H., Champion, D.C., 2007. Secular tectonic evolution of Archean continental crust: interplay between horizontal and vertical processes in the formation of the Pilbara Craton, Australia. Terra Nova 19, 1-38.

van Thienen, P., Van den Berg, A.P., Vlaar, N.J., 2004. Production and recycling of oceanic crust in the early Earth. Tectonophy. 386, 41-65.

Wang, H., van Hunen, J., Pearson, D.G., 2018. Making Archean cratonic roots by lateral compression: A two-stage thickening and stabilization model. Tectonophy. 746, 562-571.

Weller, M.B., Lenardic, A., 2012. Hysteresis in mantle convection: Plate tectonics systems. Geophys. Res. Lett. 39, doi:10.1029/2012GL051232.

Zeh, A., Gerdes, A., Barton, J.M., 2009. Archean accretion and crustal evolution of the Kalahari Craton—the zircon age and Hf isotope record of granitic rocks from Barberton/Swaziland to the Francistown Arc. J. of Petrology 50, 933-953.